Dynamics of Ultrafast Intramolecular Charge Transfer with 4-(Dimethylamino)benzonitrile in Acetonitrile†

Sergey I. Druzhinin,*,‡ Nikolaus P. Ernsting,§ Sergey A. Kovalenko,*,§ Luis Pérez Lustres,§ Tamara A. Senyushkina,§ and Klaas A. Zachariasse*,‡

Max-Planck-Institut für biophysikalische Chemie, Spektroskopie und Photochemische Kinetik, 37070 Göttingen, Germany, and Institut für Chemie, Humboldt Universität zu Berlin, Brook-Taylor Strasse 2, 12489 Berlin, Germany

Received: August 11, 2005; In Final Form: September 30, 2005

The kinetics of the intramolecular charge-transfer (ICT) reaction of 4-(dimethylamino)benzonitrile (DMABN) in the polar solvent acetonitrile (MeCN) is investigated by fluorescence quantum yield and picosecond time-correlated single photon counting (SPC) experiments over the temperature range from −45 to +75 °C, together with femtosecond $S_n \leftarrow S_1$ transient absorption measurements at room temperature. For DMABN in MeCN, the fluorescence from the locally excited (LE) state is strongly quenched, with an unquenched to quenched fluorescence quantum yield ratio of 290 at 25 °C. Under these conditions, even very small amounts of the photoproduct 4-(methylamino)benzonitrile (MABN) severely interfere, as the LE fluorescence of MABN is in the same spectral range as that of DMABN. The influence of photoproduct formation could be overcome by a simultaneous analysis of the picosecond and photostationary measurements, resulting in data for the activation barriers E_a (5 kJ/mol) and E_d (32 kJ/mol) of the forward and backward ICT reaction as well as the ICT reaction enthalpy and entropy: ΔH (−27 kJ/mol) and ΔS [−38 J/(mol K)]. The reaction hence takes place over a barrier, with double-exponential fluorescence decays, as to be expected in a two-state reaction. From femtosecond transient absorption down to 200 fs, the LE and ICT excited state absorption (ESA) spectra of DMABN in *n*-hexane (LE) and in MeCN (LE and ICT) and also of 4-aminobenzonitrile in MeCN (LE) are obtained. For DMABN in MeCN, the quenching of the LE and the rise of the ICT ESA bands occurs with a single characteristic time of 4.1 ps, the same as the ICT reaction time found from the picosecond SPC experiments at 25 °C. The sharp ICT peak at 320 nm does not change its spectral position after a pump−probe delay time of 200 fs, which suggests that large amplitude motions do not take place after this time. The increase with time in signal intensity observed for the LE spectrum of DMABN in *n*-hexane between 730 and 770 nm, is attributed to solvent cooling of the excess excitation energy and not to an inverse ICT → LE reaction, as reported in the literature.

Introduction

The structural and dynamical aspects of the intramolecular charge transfer (ICT) taking place with 4-(dimethylamino)-benzonitrile (DMABN) and related molecules have been under investigation since 1959, from an experimental[1−11] as well as more recently from a computational[12−19] point of view. After the discovery of the dual fluorescence of DMABN in polar solvents,[1] consisting of emissions from an initially prepared so-called locally excited (LE)[20] and an ICT state, Lippert et al. primarily focused their studies on the spectroscopy and kinetics of this reaction. Starting from 1973,[21] special attention was devoted to the molecular structure of the ICT state, leading to the introduction of a series of reaction models characterized by the structure of the ICT state. The following suggestions have appeared for the structural and molecular nature of the red-shifted second emission band (ICT state) of DMABN and its dual fluorescent derivatives, in the approximate order of their appearance as a model: excimer,[22] Rydberg state,[9,23] protonated molecule,[24] ICT state with perpendicularly twisted amino and benzonitrile moieties (TICT),[25] exciplex with a solvent molecule,[28] hydrogen bonded species in the ground state,[27] ICT state with pyramidalized amino group (WICT),[28] ICT state with a rehybridized nonlinear C−CN group (RICT)[29] and planar ICT state (PICT).[30−34] The essential difference between the TICT and the other ICT models for molecules such as DMABN, consists of the absence of electronic coupling between the amino and benzonitrile groups in the TICT state (principle of zero electronic overlap),[9,35] whereas in WICT, RICT, and PICT, the electron donor (D) and acceptor (A) substituents of DMABN are both electronically coupled to the phenyl group.

The support for the TICT model was mainly derived from an interpretation of the photophysical behavior of model compounds in which rotation of the amino group was prevented, or in which a large amino twist angle was already present in the electronic ground state S_0.[9] Experimental evidence based on such model compounds considered to support the TICT structure has, however, recently been shown to be inconclusive, as efficient ICT is observed with the planarized molecules 1-*tert*-butyl-6-cyano-1,2,3,4-tetrahydroquinoline (NTC6) and fluorazene.[11,36] These experiments make clear that the formation of a

† Part of the special issue "Jürgen Troe Festschrift".

* Corresponding author. Fax: +49-551-201-1501. E-mail: S.I.D., sdruzhi@gwdg.de; S.A.K., skovale@chemie.hu-berlin.de; K.A.Z., kzachar@gwdg.de.

‡ Max-Planck-Institut für biophysikalische Chemie, Spektroskopie und Photochemische Kinetik.

§ Humboldt Universität zu Berlin.

10.1021/jp054496o CCC: $33.50
Published on Web 11/09/2005

TICT structure is not required for excited state charge transfer in aminobenzonitriles and *N*-phenylpyrroles. In support of this conclusion, it has been found by picosecond X-ray analysis that the ICT state of crystalline 4-(diisopropylamino)benzonitrile (DIABN), with a fluorescence spectrum similar to that in *n*-hexane solution, has an effectively planar structure.[37] It was hence concluded that in the rigidized planar model compounds the occurrence of ICT is prevented by their structural differences with DMABN. These differences generally lead to an increase of the energy gap $\Delta E(S_1,S_2)$ between the S_1 and S_2 excited singlet states, such as in the case of 1-methyl-6-cyano-1,2,3,4-tetrahydroquinoline (NMC6).[10,36]

Apart from the structural aspects of the ICT reaction of D/A molecules, its time dependence has been the subject of many investigations. The first study of the dynamics of the ICT reaction for a dual fluorescent 4-aminobenzonitrile in a strongly polar aprotic solvent such as acetonitrile (MeCN) was made by employing oxygen quenching under high pressure (up to 100 atm) measured by phase fluorometry.[38] From these experiments, carried out with the DMABN derivative 2-methyl-4-(dimethylamino)benzonitrile, a time of 11 ps was deduced for the reaction from the LE precursor to the ICT state having a lifetime of 4.5 ns. By a direct measurement of the LE and ICT fluorescence decays of DMABN in MeCN (12 ps full width at half-maximum (fwhm) of the laser pulse), a 13 ps decay for LE and a 14 ps ICT rise time was obtained.[39] From similar streak camera experiments (20 ps pulse fwhm) pulse-limited LE decay and ICT rise times smaller than 10 ps and a decay time τ_1(ICT) of 3.7 ns were observed.[40]

By using time-correlated single photon counting (SPC) with picosecond laser excitation (30−40 ps fwhm and deconvolution),[41] double-exponential LE and ICT decays with a shortest decay time τ_2 of 6 ps were reported for DMABN in MeCN at 25 °C,[42] a time which also was found by streak camera experiments with a 4 ps time response.[43−45] From an investigation of the LE and ICT decay times of DMABN in a series of alkyl cyanides (*n*-undecyl cyanide (UnCN) to MeCN),[45,46] it was then known to us, however, that the correct decay time τ_2 of DMABN in MeCN must be shorter than 6 ps, as this time was already obtained with DMABN in the less polar solvents *n*-propyl cyanide (PrCN) and ethyl cyanide (EtCN), whereas τ_2 continuously decreases with increasing solvent polarity from UnCN to PrCN.[46] Such a decrease has also been found with several D/A molecules in other solvent families and solvent mixtures.[47−50]

To determine the correct shortest decay time τ_2 for DMABN in MeCN, $S_n \leftarrow S_1$ excited state transient absorption measurements were undertaken with DMABN in MeCN at room temperature,[51] resulting in a time τ_2 of around 4 ps. This value was then used as a guideline for the analysis of the time-resolved IR measurements of DMABN in MeCN, from which a charge-transfer time $\tau_2 = 4.0 \pm 0.5$ ps was found,[52] by tracking the downshifted CN stretching mode. Similar IR measurements later resulted in a somewhat longer ICT time τ_2 of 6.4 ps.[53,54]

From double-exponential fluorescence decays of DMABN in MeCN at room temperature, obtained by time-resolved area-normalized emission spectroscopy (TRANES) based on SPC measurements with an instrument response function of ∼40 ps, the decay times $\tau_2 = 10 \pm 5$ ps and $\tau_1 = 3.00 \pm 0.05$ ns were determined.[55] More recently,[56] streak camera measurements (system response function of ∼30 ps), led for the LE fluorescence of DMABN in MeCN at room temperature to a decay time τ_2 of 7 ps, a time τ_1 of 2.6 ns and a τ_2/τ_1 amplitude ratio *A* of 33. The ICT emission showed a rise time equal to τ_2(LE), whereas 2.9 ns was found for τ_1(ICT), slightly longer than τ_1(LE).

It is seen from the data presented above that ICT reaction times τ_2 between 4 and 7 ps have lately been obtained for DMABN in MeCN at room temperature, whereas values between 2.6 and 4.5 ns were found for τ_1, with amplitude ratios *A* between 10 and 99.[38−42,43,50,52,54,56] This insufficient accuracy of τ_2, τ_1, and *A*, obviously makes an adequate determination of the ICT kinetics impossible.[4] Therefore, the present investigation was undertaken. It should be noted that because of the formation of photoproducts with fluorescence decay times of a few nanoseconds, not only the precise evaluation of τ_1 but also that of τ_2 and consequently of *A* is affected.[42] This photoproduct leads to a lowering of *A*, indicating that the measurements with the largest *A* values will be the most reliable.

Besides the studies in dilute solution, numerous investigations have been published for DMABN in molecular jets. Whereas jet-cooled DMABN under isolated molecule conditions does not show ICT fluorescence, an anomalous red-shifted additional emission band appears for its dimers and higher self-complexes.[57] From the first jet experiments with DMABN/MeCN solvent clusters it was found that the 1:1 complex does not undergo an ICT reaction.[58] In contrast, Bernstein et al. concluded that an ICT reaction in DMABN/MeCN (two clusters of different geometry) is induced by only one properly oriented solvent molecule, namely that on top of the aromatic ring.[59] In another publication it was reported that this new red-shifted emission band originates from excitation of weakly bound ground state self-complexes and that no evidence for ICT emission could be detected with MeCN clusters.[60]

From a cluster size determination by time-of-flight mass spectrometry, Brutschy et al. found that dual fluorescence (ICT + LE) only is observed with jet-cooled DMABN, when it is complexed with a minimum of five MeCN molecules.[61] Recent jet experiments of Saigusa et al. with DMABN/MeCN as a function of cluster size *n* led to the conclusion, however, that there is no significant red shift in the fluorescence spectra (i.e., no ICT reaction) on excitation near the S_1 electronic origin, irrespective of cluster size.[62] As the excitation energy increases, a red-shifted fluorescence resembling the ICT emission band for clusters with $n \geq 5$ appears. It was concluded that the cluster temperature is too low for the ICT reaction to proceed without excess excitation energy.[62,63]

In a number of computational approaches, the energetics of the LE → ICT reaction of DMABN has been calculated.[18,19,64−72] In the following, the calculated reaction barriers and reaction energies for the ICT reaction of DMABN in the gas phase as well as in polar solvents such as MeCN are discussed (see Table S1 in Supporting Information). For the activation energy E_a in the gas phase, barriers between 10 and 76 kJ/mol have been computed, whereas considerably lower barriers were calculated for MeCN: from zero (barrier-free) to 21 kJ/mol. A large variation is also encountered in the results of the calculations for the reaction energy ΔE. In the gas phase, the reaction is generally found to be endothermic (except for a ΔE of −2 kJ/mol, or −58 kJ/mol before correction, in ref 18), between effectively zero (−2 kJ/mol) and +75 kJ/mol. In MeCN, the LE → ICT reaction then becomes exothermic, with a ΔE between −6 and −58 kJ/mol. It thus appears that, in the gas phase as well as in MeCN, the computations presently lead to vastly different results. In the most recent calculations,[72] characterizing the adiabatic S_1 equilibration path between the LE and ICT states, $E_a = 76$ kJ/mol and $\Delta E = +10$ kJ/mol for

the ICT reaction of DMABN in the gas phase have been reported. In view of the different results discussed in this section, an accurate experimental determination of the LE → ICT barrier E_a and enthalpy difference ΔH for the ICT reaction of DMABN seems to be important, to serve as a guideline for future computational efforts.

Calculations on the reaction pathway of the ICT reaction of DMABN in MeCN and methanol were presented by Hynes and his associates.[65−67] These calculations started from the molecular structure of DMABN obtained by Roos et al.,[12] and assumed a TICT structure for the ICT state. The simulation includes direct frictional damping on the ICT reaction (TICT) and solvent coordinates and resulted in a reaction time of 6.5 ps for DMABN in MeCN, in good agreement with the experimental value of 4−7 ps.[50,51] It was also concluded that the ICT reaction has an early transition state, resembling the LE state.[67]

The calculated reaction barriers E_a and ICT formation energies ΔE are to be compared with available experimental data. Such data are not available for DMABN in the gas phase, and in solution, values for E_a and ΔE are scarse.[4,41,47,73] An experimental reaction free energy ΔG of −5 kJ/mol and a reaction barrier E_a of 13 kJ/mol has been determined for DMABN in *n*-propyl cyanide among other alkyl cyanides.[47] For DMABN in a series of protic and aprotic polar solvents including alkyl cyanides, experimental reaction enthalpies ΔH between −23.8 (methanol) and −3.8 (*n*-pentyl cyanide) kJ/mol were found with reaction barriers E_a between 21 (decanol) and 6.3 (ethyl cyanide) kJ/mol. As E_a was equal to or smaller than the solvent viscosity barrier, it was concluded that the intrinsic barrier of the ICT reaction is equal to zero: a so-called barrierless reaction.[73b] With DMABN in toluene, the following thermodynamic parameters were determined: $\Delta H = -10$ kJ/mol and $E_a = 7$ kJ/mol.[4] In MeCN, such data are not available for DMABN, but only for a number of its derivatives. For the 4-aminobenzonitriles with an *n*-membered heterocyclic ring PnC in MeCN, the activation energies are 13.5 kJ/mol (P4C), 8.0 kJ/mol (P5C), 6.6 kJ/mol (P6C), and 4.7 kJ/mol (P7C), with the corresponding ICT stabilization enthalpies, $-\Delta H$, of 15 kJ/mol (P4C) and 16 kJ/mol (P5C).[41] The present investigations with DMABN in MeCN are therefore in part undertaken to obtain reliable data for ΔH and E_a in this solvent.

Several authors are of the opinion[3,9,18,64,73−75] that the ICT reaction of DMABN in polar solvents such as MeCN is barrierless and that the multiexponential (sometimes called "nonexponential kinetics") fluorescence decays they observe are a logical consequence of this situation and are not a sign of experimental problems,[30,77] such as photoproduct formation. We have, however, reported that the LE and ICT decays of DMABN and several other dual fluorescent derivatives are double-exponential over extensive temperature ranges, clearly showing that a simple kinetic scheme with two excited states LE and ICT is fully applicable.[4,20,30,32,41,42] The ICT activation energies E_a determined from these measurements indicate that the ICT reactions can not be classified as being barrierless. Only upon prolonged irradiation does a deviation from double-exponential LE and ICT decays starts to appear.[30,77]

In the present paper we report on the analysis of fluorescence decays of DMABN in the strongly polar aprotic solvent MeCN and in the nonpolar *n*-hexane, for comparison. The decays are measured by the SPC method with a laser system having a response function of ∼19 ps and a time resolution better than 3 ps.[11,20,36] To extend this time resolution down to 200 fs, S_1-S_n transient absorption experiments are carried out. The LE and ICT fluorescence SPC decays of DMABN in MeCN are measured over a large temperature range, from +75 to −45 °C, close to the melting point of the solvent. The results of these measurements are combined with photostationary LE and ICT fluorescence measurements (quantum yields and spectra). In addition, the impact of photochemical product formation on the data analysis is discussed.[77]

Experimental Section

Molecules and Solvents. DMABN was synthesized from 4-bromo-*N*,*N*-dimethylaniline (Aldrich) in a reaction with CuCN.[78] ABN was obtained from Aldrich. For these molecules, HPLC was the last purification step. The solvent acetonitrile (MeCN, Merck, Uvasol) was chromatographed over Al_2O_3, whereas *n*-hexane (Merck, Uvasol) was used as received. The solutions, with an optical density between 0.4 and 0.6 at the maximum of the first band in the absorption spectrum, were deaerated by bubbling with nitrogen for 15 min.

Absorption and Fluorescence Spectra. The absorption spectra were run on a Cary 500 spectrometer. The fluorescence spectra were measured with quantum-corrected Shimadzu RF-5000PC, ISA-SPEX Fluorolog 3-22 or (modified)[79] Fluoromax 3 spectrofluorometers. The fluorescence quantum yields Φ_f, with an estimated reproducibility of 2%, were determined with quinine sulfate in 1.0 N H_2SO_4 as a standard ($\Phi_f = 0.546$ at 25 °C),[80] with equal optical density at the excitation wavelength. The difference in refractive index between the standard solution and the solvent was not taken into account. The fluorescence quantum yield data are corrected for the temperature dependence of the optical density of the solution by measuring the absorption spectrum of DMABN as a function of temperature.

In the determination of the temperature dependence of Φ_f, the change in optical density with temperature and its nonlinear dependence on fluorescence intensity were accounted for by using absorption spectra measured over the relevant temperature range.

Fluorescence Decays and Femtosecond Transient Absorption. The fluorescence decay times were obtained with a picosecond laser (λ_{exc}: 276 nm) single photon counting (SPC) setup described elsewhere.[51,96] The picosecond laser system (excitation wavelength λ_{exc}: 276 nm) consists of a mode-locked titanium-sapphire laser (Coherent, MIRA 900F) pumped by an argon ion laser (Coherent, Innova 415). The instrument response function of the laser SPC system has a fwhm of 19 ps. Two time ranges are routinely measured simultaneously (0.5 and 10 ps/channel, in 1200 and 1800 effective channels, respectively). The estimated reproducibility is better than 10% for the ps decay times and around 2% for the nanosecond decays.

The femtosecond transient absorption setup has been described in detail elsewhere.[81,82] DMABN in *n*-hexane or acetonitrile at room temperature (∼22 °C) were excited with 1 μJ, ∼70 fs pulses at 290 or 266 nm. The pump-induced transient absorption signal was monitored with a supercontinuum probe in the range 265−680 nm or 330−1080 nm. The net sample thickness in the flow-cell was 0.4 mm. The optical density of the sample was 0.7 at the excitation wavelength. After probing the sample, the supercontinuum was dispersed and registered on a photodiode array (512 pixels) with a 1.5 nm spectral resolution. The recorded transient spectra were time-corrected for the chirp of the supercontinuum.[81] The pump−probe cross-correlation time τ_{cc} was in the range 110−140 fs, being shorter in the UV and longer in the red part of the spectrum, due to group velocity mismatch between pump and probe. The experiments, with a time resolution of 30 fs, were carried out at magic angle, unless otherwise indicated.

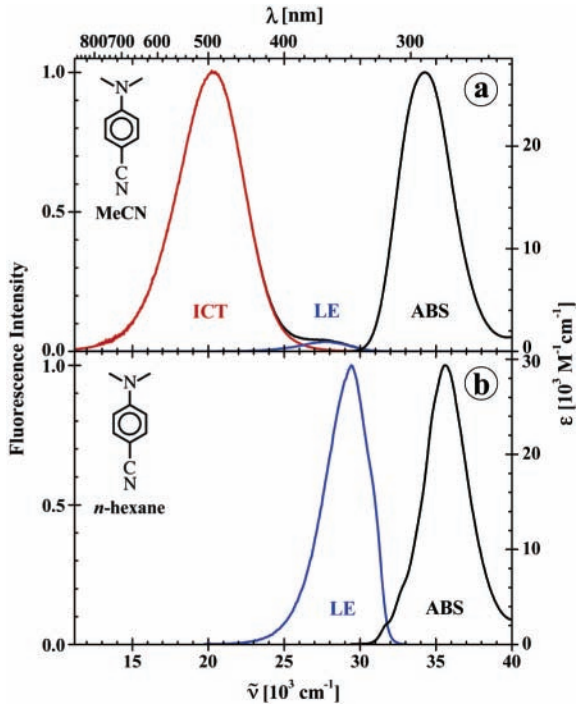

Figure 1. Fluorescence and absorption spectra of 4-(dimethylamino)-benzonitrile (DMABN) in (a) acetonitrile (MeCN) and (b) in *n*-hexane at 25 °C. The molar extinction coefficients are indicated on the right-hand axis. The fluorescence spectrum of DMABN in MeCN (a) is separated into its locally excited (LE) and intramolecular charge-transfer (ICT) components, by using the LE fluorescence spectrum of 4-(methylamino)benzonitrile (MABN). Excitation wavelength $\lambda_{exc} = 267$ nm.

The parameters for the ICT reaction and the other photophysical processes of DMABN in MeCN were obtained by a global nonlinear least-squares method,[83] with the sum of the weighted squares of the residuals $S = \sum_j \sum_i w_{ij}(y_{ij} - y_{ij}^{exp})^2$ as the target function. In the expression for S, w is the weighting factor of the response function y. The response functions y employed here are (a) the first 700 ps of the LE fluorescence decays, of which only the short component τ_2 is used and (b) the LE and ICT fluorescence quantum yields Φ(LE) and Φ'(ICT). The index j refers to the response functions, the index i counts the experimental points for each response function and "exp" indicates that the quantity is an experimental value. For a fluorescence decay the factor $w = y^{-1}$. In the data set of DMABN in MeCN collected over the temperature range from −45 to +75 °C, consisting of LE and ICT fluorescence decays and LE and ICT fluorescence quantum yields at 13 temperatures over this range, the total weight of Φ(LE) and Φ'(ICT) is adjusted in a such way that their total contribution to S is about the same as that of two fluorescence decay curves.

Results and Discussion

Fluorescence and Absorption Spectra in Acetonitrile and *n*-Hexane. The fluorescence spectrum of DMABN in acetonitrile (MeCN) at 25 °C (Figure 1a) consists of two components: a minor LE emission with a maximum at 27 700 cm^{-1} and a predominant red-shifted ICT band peaking at 20 310 cm^{-1}, with an ICT/LE fluorescence quantum yield ratio Φ'(ICT)/Φ(LE) of 39.5. For the spectral separation of these contributions to the dual fluorescence spectrum, the single LE emission band of 4-(methylamino)benzonitrile (MABN) is used, which does not undergo an ICT reaction under any condition of solvent polarity or temperature; see Figure S1 in Supporting Information.[4,30,32,83,84] The LE and ICT fluorescence quantum yields Φ of DMABN in MeCN are relatively small: 0.00076 for Φ(LE) and 0.030 for Φ'(ICT); see Table 1. The LE fluorescence is strongly quenched, with an unquenched to quenched fluorescence quantum yield ratio Φ_0(LE)/Φ(LE) of 290 at 25 °C. In this ratio Φ_0(LE) is the quantum yield of DMABN in the absence of an ICT reaction; see eq 3 and Table 4, below.

TABLE 1: Data for DMABN in Acetonitrile (MeCN) or in *n*-Hexane (HEX) When Indicated[a]

$\tilde{\nu}^{max}$(ICT) (cm^{-1})	20 310
$\tilde{\nu}^{max}$(LE) (cm^{-1})	27 700
(HEX)$\tilde{\nu}^{max}$(LE) (cm^{-1})	29 430
Φ'(ICT)	0.030
Φ(LE)	0.00076
Φ'(ICT)/Φ(LE)	39.5
ϵ^{max} (M^{-1} cm^{-1}) (at 292.0 nm, 34 250 cm^{-1})	27 990
(HEX) ϵ^{max} (M^{-1} cm^{-1}) (at 280.7 nm, 35 620 cm^{-1})	29 370
$E(S_1)^{b,c}$ (cm^{-1})	29 990
(HEX) $E(S_1)^{b,c}$ (cm^{-1})	31 830
E(FC)[c] (kJ/mol)	92.7
E_a(SB)[d] (kJ/mol)	7.7
E_d(SB)[d] (kJ/mol)	30.9
ΔH(SB)[d] (kJ/mol)	−23.2

[a] Fluorescence maxima $\tilde{\nu}^{max}$(ICT) and $\tilde{\nu}^{max}$(LE), fluorescence quantum yields Φ'(ICT) and Φ(LE), extinction coefficients ϵ^{max}, energy of the S_1 state $E(S_1)$ and energy of the Franck−Condon state E(FC) at 25 °C. The activation energies E_a and E_d of the forward (k_a) and backward (k_d) ICT reactions and the enthalpy change ΔH are also listed. [b] Energy of the crossing of the normalized absorption and fluorescence spectra. [c] See eq 4. [d] Data derived from the Stevens−Ban (SB) plot in Figure 3.

TABLE 2: LE Fluorescence Decay Times τ_2 and τ_1 and Their Amplitude Ratio A for DMABN in MeCN at 25 °C (Figure 4 and eqs 5−7), from Which the Forward and Backward ICT Reaction Rates k_a and k_d as Well as the Lifetime of the ICT State τ_0'(ICT) (Scheme 1) Are Determined by Using the Lifetime τ_0 of the Model Compound MABN (See Text)

	τ_2 (ps)	τ_1 (ps)	A	τ_0 (ps)	k_a (10^9 s^{-1})	k_d (10^9 s^{-1})	τ_0'(ICT) (ps)	τ_{LC}[a] (ps)
DMABN	4.0	3800	393	3410	249	0.63	3800	1060

[a] See eq 15 and text.

TABLE 3: Thermodynamic Parameters for the ICT Reaction of DMABN in MeCN Calculated from the LE Fluorescence Decay Times τ_2 and τ_1 and Their Amplitude Ratio A, Measured as a Function of Temperature (Figure 6)[a]

	E_a (kJ/mol)	E_d (kJ/mol)	$k_a°$ (10^{12} s^{-1})	$k_d°$ (10^{12} s^{-1})	ΔH (kJ/mol)	ΔS [J/(mol K)]
DMABN	4.5	22.5	1.48	8.99	−18.0	−15.0

[a] A correction for photoproduct formation was not made.

In Figure 1b, the fluorescence and absorption spectra of DMABN in *n*-hexane at 25 °C are shown for comparison. The emission spectrum in this nonpolar solvent mainly consists of an LE fluorescence band, with only a very small ICT contribution.[32,85] From the absorption spectra in Figure 1a,b, it is seen that the energy gap $\Delta E(S_1,S_2)$ between the two lowest excited singlet states of DMABN becomes larger when going from MeCN to *n*-hexane, as discussed previously.[26] The effective absence of dual fluorescence in the latter solvent has been connected with this larger energy gap $\Delta E(S_1,S_2)$.[21,26,37]

Fluorescence as a Function of Temperature. The total dual (LE + ICT) fluorescence spectrum of DMABN in MeCN strongly changes with temperature over the range between −45 and +75 °C (Figure 2a). Between these temperatures, the ICT emission maximum $\tilde{\nu}^{max}$ (ICT) undergoes a blue shift from 19 400 to 20 800 cm^{-1}, caused by the decrease of the effective solvent polarity, from $\epsilon^{-45} = 50.2$ to $\epsilon^{75} = 30.3$.[86] Over this

TABLE 4: Kinetic (at 25 °C) and Thermodynamic Parameters for DMABN in Acetonitrile (MeCN) Obtained from a Simultaneous Analysis of Time-Resolved and Photostationary Data and Cross Sections (See Text)

τ_1 (ps)	3800
τ_2 (ps)	4.1
Φ_0(LE)[a]	0.220
Φ'_0(ICT)[b]	0.030
Φ'(ICT)/Φ(LE)	39.8
A, eq 7	516
k_a (10^9 s^{-1})	240
k_d (10^9 s^{-1})	0.47
τ'_0(ICT) (ps)	3800
k_f(LE) (10^9 s^{-1})	0.065
k'_f(ICT) (10^9 s^{-1})	0.0079
E_a (kJ/mol)	5.0 ± 0.25
E_d (kJ/mol)	32.0 ± 0.4
k_a^0 (10^{12} s^{-1})	1.83 ± 0.02
k_d^0 (10^{12} s^{-1})	186.8 ± 0.2
ΔH (kJ/mol)	−27.0 ± 0.7
ΔS [J/(mol K)]	−38[c] ± 1
E(FC)[d] (kJ/mol)	88.9
σ_{abs} (10^{-17} cm^2)[e]	4.52 at 292 nm
σ_{SE}(LE) (10^{-17} cm^2)[f]	1.62 at 364 nm
σ_{SE}(ICT) (10^{-17} cm^2)[f]	0.257 at 505 nm

[a] $\Phi_0(\mathrm{LE}) = k_f(\mathrm{LE})\tau_0$. From eq 3: LE fluorescence quantum yield without ICT reaction ($k_a = 0$); see Figure S2. [b] $\Phi'_0(\mathrm{ICT}) = k'_f(\mathrm{ICT})\tau'_0(\mathrm{ICT})$, (eq 2): ICT fluorescence quantum yield without back reaction ($k_d \ll 1/\tau'_0(\mathrm{ICT})$); see Figure S2. [c] At 25 °C, $T\Delta S = -11.4$ kJ/mol. $\Delta S = R \ln(k_a^0/k_d^0)$. [d] Equation 4. $E(S_1)$ MeCN, 29 990 cm^{-1}, $\tilde{\nu}^{max}$(ICT) 25 °C, 20 310 cm^{-1} (Table 1). [e] $S_n \leftarrow S_0$ absorption cross section. [f] Stimulated emission cross section.

temperature range, $\tilde{\nu}^{max}$ (LE) changes from 27 640 to 27 740 cm^{-1}. From these data, the dipole moments μ_e(ICT) and μ_e(LE) can be determined and will be treated separately.[77]

The ICT fluorescence quantum yield Φ'(ICT) of DMABN in MeCN (Figure 2b) monotonically increases, from 0.019 at −45 °C to 0.038 at +75 °C, whereas the much smaller LE yield Φ(LE) first slightly decreases from 0.00053 at −45 °C, reaches a minimum 0.00047 at −15 °C, and then strongly increases to 0.0025 at +75 °C. The temperature dependence of the ratio Φ'(ICT)/Φ(LE) is plotted in Figure 3; see eqs 1−3 and Scheme 1. The limiting yields $\Phi'_f(\mathrm{ICT}) = k'_f(\mathrm{ICT})\tau'_0(\mathrm{ICT})$ (eq 2) and $\Phi_0(\mathrm{LE}) = k_f(\mathrm{LE})\,\tau_0(\mathrm{LE})$ (eq 3) are obtained, respectively, when the ICT back reaction k_d can be neglected ($k_d \ll 1/\tau'_0(\mathrm{ICT})$) or ICT does not take place ($k_a = 0$); see Figure S2 in Supporting Information. In eqs 1−3 and Scheme 1, k_a and k_d are the rate constants of the forward and backward ICT reaction, τ_0(LE) and τ'_0(ICT) are the fluorescence lifetimes, and k_f(LE) and k'_f(ICT) are the radiative rate constants.

$$\frac{\Phi'(\mathrm{ICT})}{\Phi(\mathrm{LE})} = \frac{k'_f(\mathrm{ICT})}{k_f(\mathrm{LE})}\frac{k_a}{k_d + 1/\tau'_0(\mathrm{ICT})} \quad (1)$$

$$\Phi'(\mathrm{ICT}) = k'_f(\mathrm{ICT})\tau'_0(\mathrm{ICT})\frac{k_a\tau_0(\mathrm{LE})}{1 + k_a\tau_0(\mathrm{LE}) + k_d\tau'_0(\mathrm{ICT})} \quad (2)$$

$$\Phi(\mathrm{LE}) = k_f(\mathrm{LE})\,\tau_0(\mathrm{LE})\frac{1 + k_d\tau'_0(\mathrm{ICT})}{1 + k_a\tau_0(\mathrm{LE}) + k_d\tau'_0(\mathrm{ICT})} \quad (3)$$

Stevens−Ban Plot. By fitting the Stevens−Ban[87] plot of Φ'(ICT)/Φ(LE) in Figure 3 with eq 1,[4,88,89] we obtain the activation energies of the forward and backward ICT reaction (Scheme 1): $E_a = 7.7$ kJ/mol and $E_d = 30.9$ kJ/mol, i.e., $\Delta H = E_a - E_d = -23.2$ kJ/mol. It is thereby assumed that k'_f(ICT)/k_f(LE) and also τ'_0(ICT) do not depend on temperature. This assumption will be tested in a later section by direct measurement of k'_f(ICT)/k_f(LE) and τ'_0(ICT) employing time-resolved experiments. A more precise analysis of Φ'(ICT)/Φ(LE), together with data for k_a, k_d, k'_f(ICT), k_f(LE), and τ'_0(ICT) (see eq 1) coming from time-resolved experiments, is presented below.

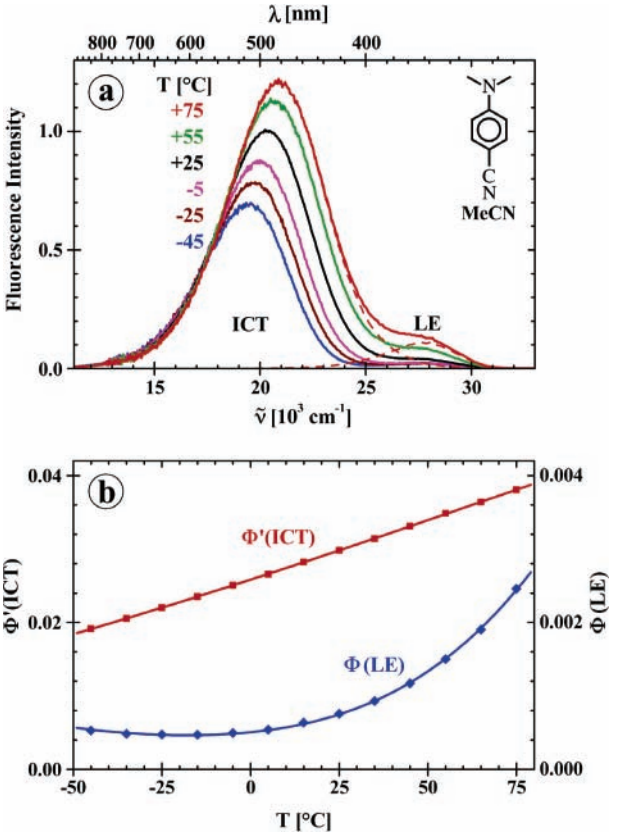

Figure 2. (a) Fluorescence spectra of 4-(dimethylamino)benzonitrile (DMABN) in acetonitrile (MeCN) as a function of temperature, from +75 to −45 °C. The total emission spectrum at 75 °C is separated into the contributions from the locally excited (LE) and intramolecular charge-transfer (ICT) states. The red shift of the ICT emission band upon cooling is caused by an increase in the solvent polarity; see text. Excitation wavelength λ_{exc} = 290 nm. (b) Separate ICT and LE fluorescence quantum yields Φ'(ICT) and Φ(LE) as a function of temperature.

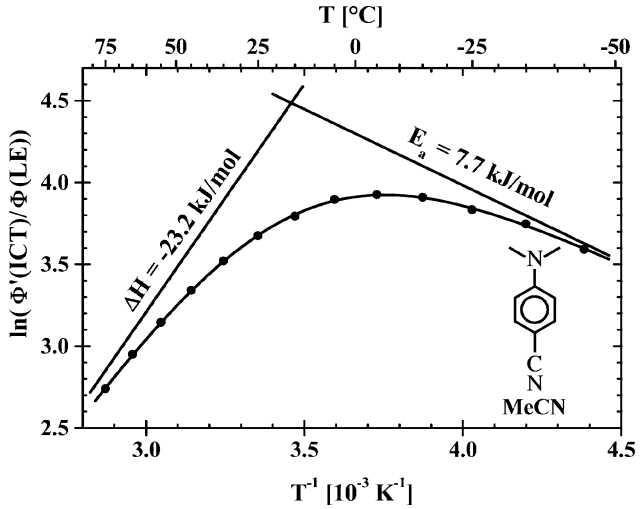

Figure 3. Stevens−Ban plot of the ICT/LE fluorescence quantum yield ratio Φ'(ICT)/Φ(LE) of 4-(dimethylamino)benzonitrile (DMABN) in acetonitrile (MeCN). From the high-temperature limit (HTL) slope the ICT reaction enthalpy ΔH is obtained, whereas the low-temperature limit (LTL) slope yields the activation energy E_a of the LE → ICT reaction.

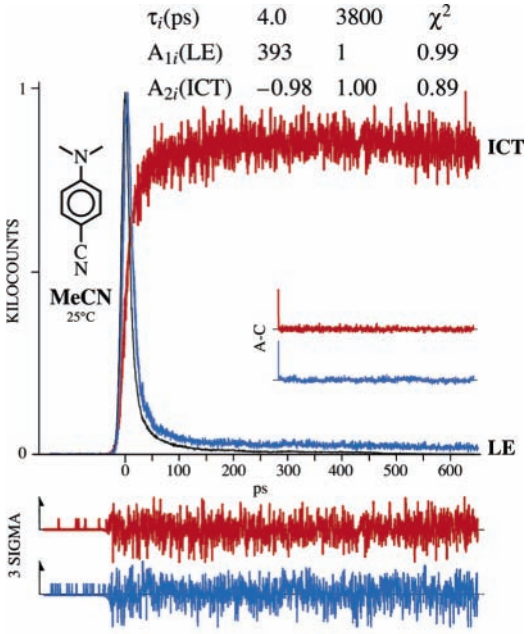

Figure 4. Double-exponential LE (350 nm) and ICT (520 nm) fluorescence decays of 4-(dimethylamino)benzonitrile (DMABN) in acetonitrile (MeCN) at 25 °C. The decay times are τ_2 and τ_1 with the corresponding amplitudes A_{1i}(LE) and A_{2i}(ICT); see eqs 5−7. The shortest decay time is listed first. The weighted deviations σ, the autocorrelation functions A−C, and the values for χ^2 are also indicated. Excitation wavelength λ_{exc}: 276 nm. Time resolution: 0.5 ps/channel with a time window of 2000 channels.

SCHEME 1

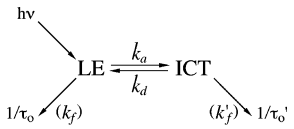

The energy difference E(FC) between the Franck−Condon state FC(ICT) reached by emission from the ICT state and the equilibrated S_0 state of DMABN in MeCN, calculated via eq 4,[4,30,41] amounts to 92.7 kJ/mol. This means that the red shift of the ICT band is for 80% caused by the strongly destabilized FC(ICT) state, an indication of a substantial structural difference between the ICT and the S_0 states.

$$E(\mathrm{FC}) = E(\mathrm{S_1}) + \Delta H - \tilde{\nu}^{\max}(\mathrm{ICT}) \tag{4}$$

where $E(S_1)$ is the energy of the S_1 state.

LE and ICT Picosecond Fluorescence Decays in MeCN at 25 °C. A global analysis of the LE and ICT fluorescence decays of DMABN in MeCN at 25 °C, with a time resolution of 0.5 ps/channel, is shown in Figure 4. These LE and ICT decays are measured at wavelengths at which either only LE (350 nm) or only ICT (520 nm) fluorescence occurs; see Figure 1. The decays i_f(LE) and i_f(ICT) are double-exponential (eqs 5 and 6), with decay times τ_2 of 4.0 ps and τ_1 of 3.80 ns (Table 2). The LE amplitude ratio $A = A_{12}/A_{11}$ (eq 7) equals 393, which

$$i_f(\mathrm{LE}) = A_{11}\exp(-t/\tau_1) + A_{12}\exp(-t/\tau_2) \tag{5}$$

$$i_f(\mathrm{ICT}) = A_{21}\exp(-t/\tau_1) + A_{22}\exp(-t/\tau_2) \tag{6}$$

$$A = A_{12}/A_{11} \tag{7}$$

means that, to a very small extent, the ICT → LE back reaction (Scheme 1) still takes place with DMABN in MeCN at room temperature. As discussed in the Introduction, times between 4 and 7 ps for τ_2 and between 2.6 and 4.5 ns for τ_1 can be found in the literature, with amplitude ratios A between 10 and 99.[38−42,43,50,52,54,56] Complications in the interpretation of the kinetic significance of the value of A,[41,77] caused by photochemical products with decay times similar to the τ_1 of DMABN, will be discussed below.

The expressions for τ_1, τ_2, and A appearing in eqs 5−7 are[4]

$$1/\tau_{1,2} = \frac{1}{2}\{(X+Y) \mp \sqrt{(X-Y)^2 + 4k_a k_d}\} \tag{8}$$

$$A = \frac{X - 1/\tau_1}{1/\tau_2 - X} = \frac{k_a k_d \tau_0^{\,2}}{(1 + k_a\tau_0 - \tau_0/\tau_1)^2} \tag{9}$$

where

$$X = k_a + 1/\tau_0 \tag{10}$$

$$Y = k_d + 1/\tau_0' \tag{11}$$

The observation that the ICT amplitude ratio $-A_{22}/A_{21}$ (Figure 4; see eq 6), is close to unity, indicates that the ICT state of DMABN is not formed by direct excitation from the ground state but originates exclusively from the initially excited LE state as the precursor (adiabatic reaction on the S_1 potential energy surface), as was first demonstrated for DMABN in toluene.[4,87] This conclusion will be substantiated by the femtosecond measurements presented in a later section.

ICT Reaction Parameters. From the decay times τ_2 and τ_1 together with the amplitude ratio A (eqs 5−7) and the lifetime τ_0 of the model compound MABN, the rate constants k_a and k_d and the lifetime τ_0'(ICT) can in principle be calculated by using eqs 12−14 (Scheme 1);[4,20,87] see Table 2. The fluorescence

$$k_a = (1/\tau_1 + A/\tau_2)/(1 + A) - 1/\tau_0(\mathrm{LE}) \tag{12}$$

$$k_d = \{(1/\tau_2 - 1/\tau_1)^2 - (2k_a + 2/\tau_0(\mathrm{LE}) - 1/\tau_1 - 1/\tau_2)^2\}/4k_a \tag{13}$$

$$1/\tau_0' = 1/\tau_1\left(1 + k_d\frac{\tau_0 - \tau_1}{1 + k_a\tau_0 - \tau_0/\tau_1}\right) \tag{14}$$

lifetime of MABN at each temperature is taken for τ_0(LE) of DMABN (Scheme 1), as dual emission is not observed with this system in MeCN (Figure S1), nor in any other solvent investigated.[4,30,32,83,84]

By deconvolution of the ICT decay by the LE decay curve as the formal excitation pulse, a single-exponential decay time τ(LC) should result when Scheme 1 is valid, equal to $1/(k_d + 1/\tau_0'(\mathrm{ICT}))$; see eq 15.[51] From the LE and ICT curves of

$$1/\tau(\mathrm{LC}) = k_d + 1/\tau_0'(\mathrm{ICT}) \tag{15}$$

DMABN in MeCN at 25 °C (Figure 4) a single-exponential LE/ICT decay is obtained, with a time τ(LC) of 1060 ps, close to the 1120 ps calculated (eq 15) from k_d and $1/\tau_0'$(ICT) in Table 2.

This observation of a single-exponential LE/ICT decay shows that there is no severe interference with fluorescence from photoproducts.[51] Nevertheless, the experimental value for τ(LC) found here is still smaller than our final result $k_d + 1/\tau_0'(\mathrm{ICT}) = 1360$ ps (see Table 4 below), due to the reduction of A caused by the presence of small amounts of photoproduct.

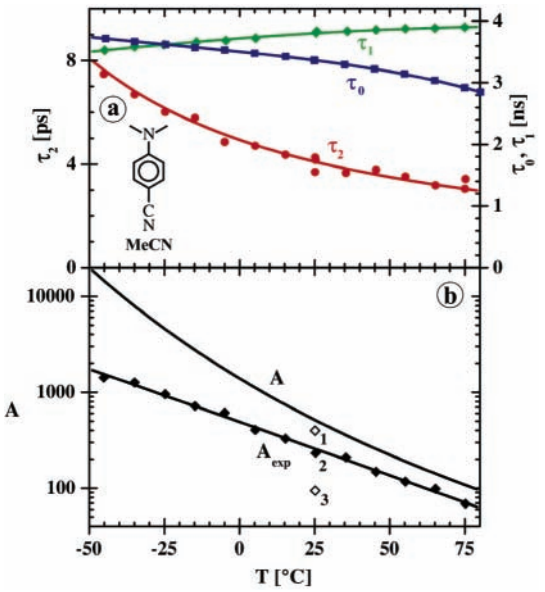

Figure 5. Plots as a function of temperature of (a) the experimental fluorescence decay times τ_2 and τ_1 (eqs 5 and 6) of 4-(dimethylamino)-benzonitrile (DMABN) and the lifetime τ_0 of 4-(methylamino)-benzonitrile (MABN) in acetonitrile (MeCN) and of (b) the experimental LE amplitude ratio A_{exp} (eq 7) of DMABN in MeCN. These values of A_{exp} have not been corrected for the effects of photoproduct formation. The curve above A_{exp} represents A as obtained from the final simultaneous analysis of time-resolved and photostationary data as a function of temperature; see text and the final results for τ_2, τ_1, and τ_0 in Figure 9. The least-squares lines through the points only serve to connect the data. The points for A_{exp} marked 1, 2, and 3 refer to consecutive experiments (see text) showing the effect of photoproduct formation.

Fluorescence Decays as a Function of Temperature. The decay times τ_2 and τ_1 as well as their amplitude ratio A of DMABN in MeCN were determined over the temperature range from −45 to +75 °C (close to the melting and boiling points of the solvent, respectively) from SPC measurements of the LE and ICT fluorescence decays. The results are depicted in Figure 5. The shortest decay time τ_2 and the ratio A come from LE decays with a time resolution of 0.5 ps/channel, whereas the nanosecond decay times τ_1 are taken from the ICT fluorescence decays with 10.4 ps/channel, which are routinely measured together with the higher resolution data. In the fitting of the LE decays, this time τ_1 is kept fixed.

With increasing temperature, τ_2 becomes smaller, from 7.7 ps at −45 °C to 3.3 ps at +75 °C (Figure 5a), with a corresponding decrease of A from around 1420 to 69 (Figure 5b). The time τ_1 does not depend strongly on temperature, changing from 3.53 ns at the lowest to 3.90 ns at the highest temperature. Note that τ_1 is in fact equal to the ICT lifetime τ_0'(ICT); see Table 2. From these data together with τ_0(MABN) (see above), the ICT rate constants k_a and k_d and also τ_0'(ICT) (eqs 12−14, Scheme 1) can again be calculated. The results are presented in Figure 6. From this Arrhenius plot, the activation energies of the forward (E_a) and backward (E_d) reaction are obtained: $E_a = 4.5$ kJ/mol, $E_d = 22.5$ kJ/mol, i.e., $\Delta H = E_a - E_d = -18.0$ kJ/mol; see Table 3. From the preexponential factors $k_a°$ and $k_d°$ in Table 2, $\Delta S = -15.0$ J/(mol K).

Reduction of LE Ratio *A* by Photoproducts. In the present case with large values for A (Figure 5b), the determination of k_a and k_d (eqs 12 and 13, Scheme 1) from τ_2, τ_1, and A, is complicated by the fact that by irradiation of DMABN the photoproduct MABN is produced,[77] which has an LE fluorescence decay time τ_0 similar to the τ_1 of DMABN: 3410 ps (τ_0) as compared with 3800 ps (τ_1) in MeCN at 25 °C (Table 2). The accumulation of this photoproduct therefore leads to an apparent decrease of A, thereby making the calculation of k_d inaccurate. This difficulty was already encountered during our earlier experiments with DMABN in MeCN,[41] where it was mentioned that the decay time analysis was complicated by photochemical product interference, as also discussed above. Although the present observation of large values for A (393 at +25 °C; 1420 at −45 °C, Figure 5b) clearly shows that this interference has now considerably been reduced (in the literature, A ranges between 10 and 99 at 25 °C; see above), the fact that A is found to depend on irradiation time of the sample (Figure 5b, consecutive points 1 (393), 2 (233), and 3 (94) at 25 °C) nevertheless shows that the experimental amplitude ratios are still affected by photoproduct formation. As a consequence, due to the fact that $k_a/k_d \cong A$ in the present case of $\tau_2 \ll \tau_1$,[4,87] a sufficiently precise calculation of k_d becomes impossible, whereas k_a and its temperature dependence can be obtained with more confidence ($k_a \cong 1/\tau_2$ when A is large);[4,87] see Table 2. It therefore obviously became necessary to adopt a different procedure for the determination of k_d. For this purpose, a simultaneous fitting of time-resolved and photostationary fluorescence data collected over a large temperature range was carried out. With the fluorescence spectra, photodecomposition can be neglected due to the much lower excitation intensity than in the case of the picosecond decays. The fitting procedure will be discussed in the following section.

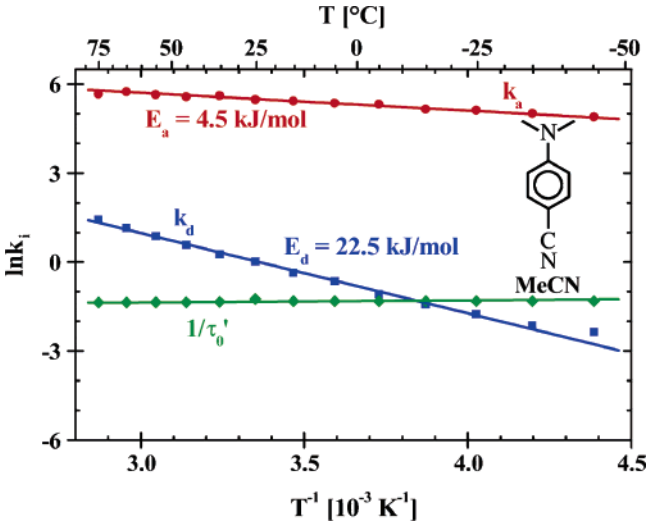

Figure 6. Arrhenius plot of the apparent rate constants k_i (k_a, k_d, and $1/\tau_0'$(ICT), in 10^9 s^{-1}) (see Scheme 1) of 4-(dimethylamino)benzonitrile (DMABN) in acetonitrile (MeCN). The data were obtained from for τ_2, τ_1, and the uncorrected value of A, taken from the experimental fluorescence decays together with the lifetime τ_0 of the model compound 4-(methylamino)benzonitrile (MABN); see text and Figure 6.

Simultaneous Fitting of Time-Resolved and Photostationary Data as a Function of Temperature. In the LE ⇄ ICT reaction (Scheme 1), six unknowns are involved: k_a, k_d, τ_0(LE), τ_0'(ICT), k_f(LE), and k_f'(ICT). To calculate these six reaction parameters, a set of six experimentally accessible and reliable independent data should be available. Five of these data come from (a) the LE and ICT fluorescence decays (τ_1, τ_2: Figure 5a), (b) the fluorescence lifetime of the model compound[4,30,32,83,84] τ_0(MABN) (Figure 5a), and (c) the LE and ICT fluorescence quantum yields Φ(LE) and Φ′(ICT); see Figure 2b. As the ratio A (eq 9), which is normally used as the sixth input in these calculations,[4,36] cannot be determined experimentally with sufficient accuracy for DMABN in MeCN due to

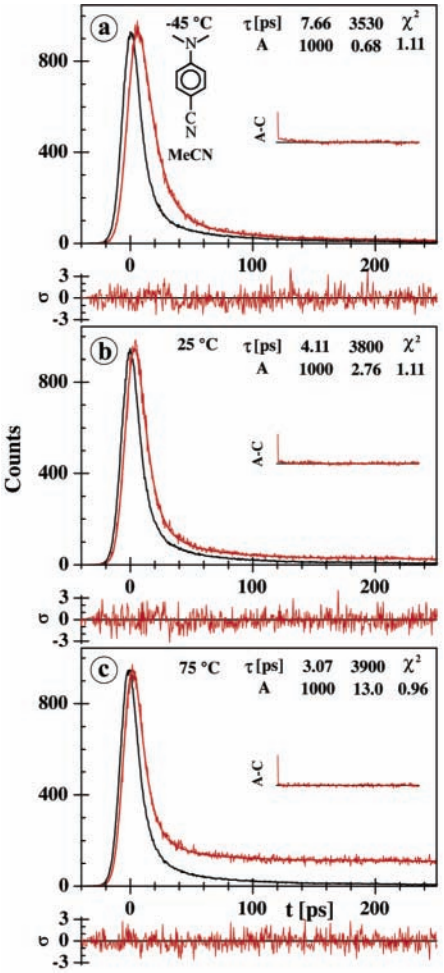

Figure 7. LE fluorescence decays of 4-(dimethylamino)benzonitrile (DMABN) in acetonitrile (MeCN) at three temperatures, obtained from the simultaneous analysis described in the text; see Figure 8. Excitation wavelength: 276 nm. Emission wavelength: 350 nm. Time resolution: 0.5 ps/channel with a time window of 1400 channels (500 shown). See caption of Figure 4.

photoproduct interference, as discussed in the previous section, an alternative source for the missing data input is required.

To achieve this goal, the LE and ICT fluorescence decays, τ_0(MABN), Φ(LE) and Φ'(ICT) were measured as a function of temperature from −45 to +75 °C (Figures 5a and 2b). Using this entire data set, a simultaneous fitting of the LE fluorescence decays i_f(LE), the main source of τ_2 (see Figure 7 and Experimental Section), together with the results for τ_1, τ_0, Φ(LE), and Φ'(ICT) was then carried out, with the following constraints. The rate constants k_a and k_d at the various temperatures, with their activation energies E_i and preexponential factors k_i^0, are defined by the Arrhenius expressions eqs 16 and 17. In addition, on the basis of the findings with the model compound MABN in MeCN (Figure S3), it is assumed that the temperature dependence of the LE radiative rate k_f(LE) can be expressed as $k_f(\mathrm{LE}) = k_f(0)n^2$ (eq 18), where n is the refractive

$$1/\tau_2 = k_a + 1/\tau_0 - \frac{k_a k_d \tau_0}{1 + k_a\tau_0 - \tau_0/\tau_1} \qquad (8a)$$

$$k_a = k_a^{\,0} \exp(-E_a/\mathrm{RT}) \qquad (16)$$

index of the solvent and $k_f(0)$ does not depend on tempperature.[83] Equations 8a and 14 were used for τ_2 and τ_0'(ICT) in the fitting procedure (see Experimental Section). Equation 8a is algebraically equivalent to eq 8. The final values for τ_2 obtained by the simultaneous fitting are presented in Figure 8, together with the input data for τ_1 and τ_0.

$$k_d = k_d^{\,0} \exp(-E_d/\mathrm{RT}) \qquad (17)$$

$$k_f(\mathrm{LE}) = k_f(0)n^2 \qquad (18)$$

When the LE and ICT fluorescence decays (τ_1,τ_2), τ_0(LE), Φ(LE), and Φ'(ICT) are measured at m different temperatures and analyzed simultaneously, 5m equations become available. With the constraints (eqs 16−18), one then has as unknowns: τ_0'(ICT) and k_f'(ICT) plus the 5 parameters k_a°, k_d°, E_a, E_d, and $k_f(0)$ in eqs 16−18, in total $2m + 5$ unknowns. Therefore, already at $m = 2$, the system is defined and can be solved by the least-squares method. In the present case $m = 13$.

ICT Reaction Parameters and Stevens−Ban Plot of DMABN in MeCN. The rate constants k_a and k_d as well as the ICT lifetime τ_0'(ICT) (eqs 12−14) resulting from this simultaneous fitting procedure are plotted as a function of temperature in Figure 9b. From these data, the activation energies E_a (5.0 kJ/mol) and E_d (32.0 kJ/mol) and the preexponential factors k_a^0 (1.8×10^{12} s^{-1}) and k_d^0 (190×10^{12} s^{-1}) are determined (eqs 16 and 17, Table 4), giving the ΔH (−27.0 kJ/mol) and ΔS [−38 J/(mol K)] for the ICT reaction. The change in enthalpy $-\Delta H$ (equal to $E_d - E_a$) of 27.0 kJ/mol obtained here for the ICT reaction of DMABN in MeCN is substantially larger than that found in the less polar solvents toluene[4b] (11.6 kJ/mol) and diethyl ether[49,89] (15 kJ/mol), as to be expected from the large polarity of MeCN ($\epsilon = 36.7$ at 25 °C) as compared with toluene ($\epsilon^{25} = 2.37$) or DEE ($\epsilon^{25} = 4.23$).[86] The activation barrier E_a of 5 kJ/mol means that the ICT process of DMABN in MeCN is not a barrierless reaction.

A comparison of the results in Tables 4 and 3 shows that, in particular the data involving the ICT → LE rate constant k_d are affected when photoproduct formation is neglected, with in that case the following not optimal results (Table 3): E_d (22.5 kJ/mol), ΔH (−18.0 kJ/mol) and ΔS [−15.0 J/(mol K)].

In Figure 9a, a fit of the Stevens−Ban plot of Φ'(ICT)/Φ(LE) is presented, using the final data for k_a, k_d, τ_0(LE), and τ_0'(ICT) (Figure 9b). A comparison with Figure 3 shows that the activation barrier E_a has now changed from 7.7 to 5.0 kJ/mol, whereas $-\Delta H$ increased from 23.2 to 27.0 kJ/mol, a smaller difference than that found between the $-\Delta H$ (18.0 kJ/mol) obtained from the fluorescence decays when the interference of photoproduct formation is not removed (Figure 6) and the final value of 27.0 kJ/mol.

Calculation of LE Amplitude Ratio A and Radiative Rate Constants k_f'(ICT) and k_f(LE). From the data for k_a, k_d, and τ_0'(ICT) obtained from the simultaneous fitting, the LE amplitude ratio A (eq 7) can now be calculated via eq 9. It is clear from Figure 5b that A is considerably larger than the directly measured (i.e., uncorrected) experimental values, which difference is caused by photoproducts fluorescing at the spectral position at which the LE fluorescence decays are measured, as discussed above. For example, at +75, +25, and −45 °C the following A values are calculated (uncorrected values in parentheses): 108 (69), 516 (393), 14485 (1420); see Figure 5b.

The experimental information allowing the determination of k_d in the simultaneous analysis is mainly contained in Φ(LE), eq 3. Even with an amplitude ratio $A = A_{12}/A_{11}$ (eq 7) of 516 at 25 °C (Figure 5b), the contribution $\tau_1/(\tau_1 + A\tau_2)$ of τ_1 to the total integrated LE fluorescence intensity Φ(LE) still equals 0.642, due to the large difference between τ_2 and τ_1 ($\tau_1/\tau_2 =$

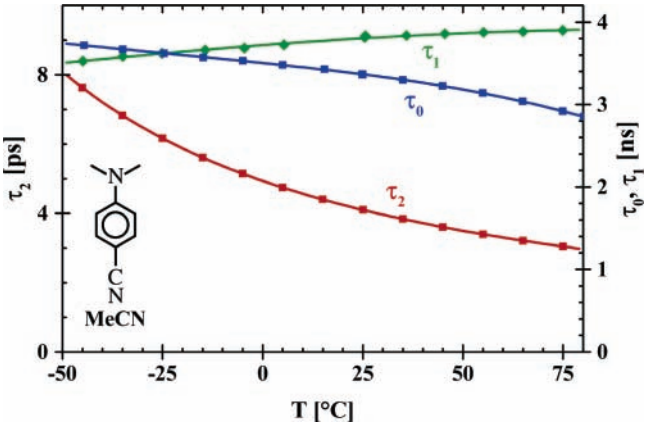

Figure 8. Plot of the final fluorescence decay time τ_2 (eq 8a) for 4-(dimethylamino)benzonitrile (DMABN) in acetonitrile (MeCN) as a function of temperature, together with τ_1 and τ_0. These data come from the simultaneous analysis of the LE fluorescence decays, τ_1, τ_0, Φ(LE), and Φ'(ICT); see text. The decay times τ_0 are the fluorescence lifetimes of the model compound 4-(methylamino)benzonitrile (MABN). In this procedure, the effect of photoproduct formation on A is removed; see Figure 5b. The lines through the points are calculated from the final results for k_a, k_d, τ_0(LE), and τ_0'(ICT) (eqs 2, 3, 8, and 14).

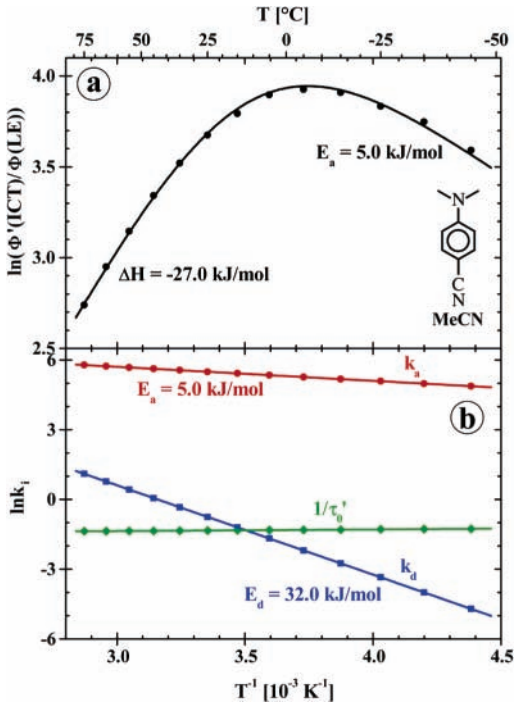

Figure 9. (a) Fit of the Stevens−Ban plot (see eq 1 and Figure 3) obtained by using the final results for k_a, k_d, τ_0'(ICT), k_f'(ICT), and k_f(LE). (b) Arrhenius plot of the final rate constants k_i (k_a, k_d, and $1/\tau_0'$(ICT), in 10^9 s^{-1}) (see Scheme 1) of 4-(dimethylamino)benzonitrile (DMABN) in acetonitrile (MeCN). The data were obtained from a simultaneous analysis of fluorescence decays and photostationary experiments; see text, Table 4 and Figures 2b and 8.

925, Figure 7b). This means that 64% of the LE decay is associated with τ_1 and that therefore A ($\approx k_a/k_d$) and hence k_d is firmly established experimentally. Note in this connection that the double-exponential character of the LE fluorescence decay (eq 5) is caused by the ICT back reaction k_d.

Similarly, the radiative rate constants k_f'(ICT) and k_f(LE) as well as their temperature dependence are now available from the simultaneous fitting. It is seen from Figure 10 that k_f'(ICT), k_f(LE), and hence k_f'(ICT)/k_f(LE) do depend on temperature. The temperature dependence of k_f(LE) is caused by the solvent

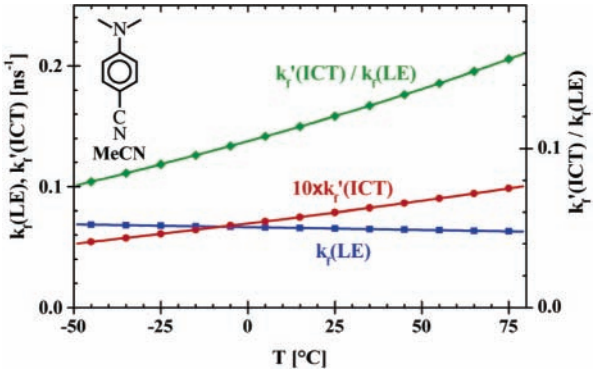

Figure 10. Radiative rate constants k_f(LE) and k'_f(ICT) for DMABN in acetonitrile (MeCN) as a function of temperature.

refractive index (eq 18), whereas for k_f'(ICT) eq 18 apparently does not hold, different from our initial assumption (Figure 3) that the ratio k_f'(ICT)/k_f(LE) is temperature independent.

Influence of Temperature Dependence of Solvent Polarity on ICT Activation Barrier. The solvation energy, calculated via eq 19,[90] of the ICT state of DMABN in MeCN (μ_e(ICT) = 17 D),[10] changes by 2.24 kJ/mol between +75 and −45 °C, whereas that of the LE state changes by 0.87 kJ/mol, a difference of 1.37 kJ/mol. In this calculation, the following data are used: μ_e(LE) = 10.6 D, μ_e(ICT) = 17 D, and ρ = 4.20 Å.[10]

$$\Delta G_{solv} = -N\mu^2(\epsilon - 1)/\rho^3(2\epsilon + 1) \qquad (19)$$

where N is the Avogadro number, μ is the dipole moment, ρ is the Onsager radius, and ϵ is the dielectric constant.

When the transition state for the LE → ICT reaction has the character of the final ICT state (late transition state),[51] this means that the effective activation barrier E_a will become lower with decreasing temperature, as the dipole moment μ_e(LE) of the LE state (10.6 D) is smaller than μ_e(ICT).[10] A similar behavior has been found previously.[47−49] The value of 5 kJ/mol determined here (Figure 9b) should hence be considered as a mean value of E_a over the temperature range between +75 and −45 °C; i.e., when taking the uncertainties in the experiments and in the solvation energy calculations into account, E_a decreases from 6 to 4 kJ/mol between +75 and −45 °C.[91,92]

Transient Absorption Spectra of DMABN and ABN in *n*-Hexane and Acetonitrile. The first transient absorption spectrum of DMABN in MeCN was published by Okada et al.[93] These authors probed the range 315−480 nm at a pump−probe delay time of 100 ps. The transient spectrum consists of a main maximum at 325 nm and a smaller one at around 400 nm. At the delay of 100 ps, it is the spectrum of the ICT state. Parker et al. measured a similar spectrum (380−600 nm) at a delay time of 50 ps, with a maximum at 420 nm.[94] In *n*-hexane (no ICT, see above) at 2 ps, the transient absorption spectrum (440−740 nm) of the LE state of DMABN has maxima at 460, 525, and 710 nm, and largely the same LE spectrum was obtained at a 3 ps delay in ethanol.[85] The LE transient spectrum of 4-aminobenzonitrile (ABN), in MeCN as well as in *n*-hexane, is comparable in shape to that for the LE state of DMABN in the last solvent.[7]

To expand the time range of our investigation of the ICT reaction with DMABN in MeCN down to 100 fs, femtosecond transient absorption measurements were performed at room temperature (~22 °C). For comparison, such experiments were also carried out with DMABN in *n*-hexane, and also with ABN in MeCN and *n*-hexane. The transient absorption spectra of ABN in *n*-hexane and MeCN and of DMABN in *n*-hexane are treated

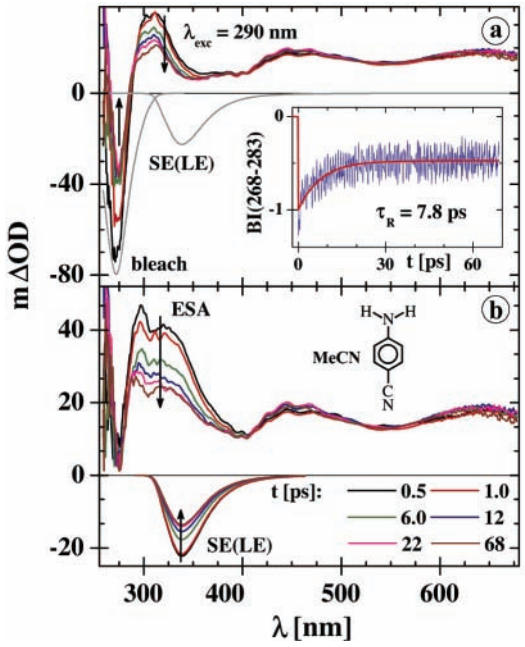

Figure 11. (a) Transient absorption spectra (260−680 nm) of 4-aminobenzonitrile (ABN) in acetonitrile (MeCN) for pump−probe delay times between 0.5 and 68 ps. Pump wavelength was $\lambda_{exc} = 290$ nm and the probe was parallel polarized. The bleach band and the stimulated LE emission SE(LE) are also shown. (b) Time development of the excited state absorption (ESA) and SE(LE) spectra. The decay of the band integral BI(268−283) over the bleach band between 268 and 283 nm, inset in (a), comes from rotational diffusion with a time constant $\tau_R = 7.8$ ps. The spectral evolution of the various bands is indicated with an arrow. As an ICT reaction does not occur, (b) is the ESA spectrum of the LE state. mΔOD is the change in optical density/1000.

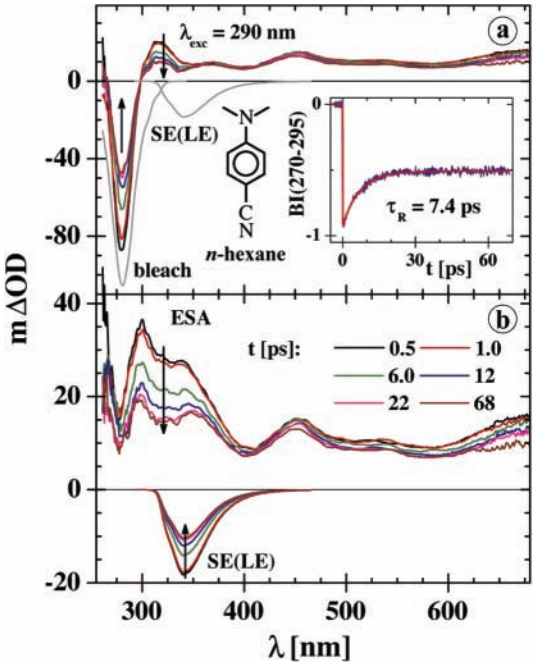

Figure 12. (a) Transient absorption spectra (260−680 nm) of 4-(dimethylamino)benzonitrile (DMABN) in *n*-hexane, for pump−probe delay times between 0.5 and 68 ps. The pump wavelength was $\lambda_{exc} = 290$ nm and the probe was parallel polarized. The bands for bleach and stimulated LE emission SE(LE) are also shown. (b) Time development of the excited state absorption (ESA) and SE(LE) spectra. The band integral BI(270−295) over the bleach band between 270 and 295 nm decays with a time constant $\tau_R = 7.4$ ps, inset (Table 5), caused by rotational diffusion of DMABN. A weak signal evolution in other spectral regions, BI(300−350) and BI(450−600), with a similar decay time is likewise assigned to rotational diffusion. The spectral evolution of the various bands is indicated with an arrow. As an ICT reaction does not occur with DMABN in *n*-hexane, the ESA spectrum in (b) is that of the LE state. mΔOD is the change in optical density/1000.

first, as in these systems an ICT state is absent (ABN) or kinetically insignificant (DMABN) and the spectra therefore are from the LE state.[4,30,32,83,84] In this manner, the LE and the ICT components of the overall transient absorption spectrum of DMABN in MeCN can be identified.

Decomposition of the Transient Spectra. Transient absorption spectra generally consist of contributions from ground state bleaching (BL), excited state absorption (ESA) and stimulated emission (SE). When a two-state kinetics is involved, such as in Scheme 1, each of the two excited states (LE and ICT) have their ESA and SE bands. For the decomposition of the overall transient spectra, it is assumed that the BL contribution is essentially independent of time at magic angle excitation. The spectral shape of the BL band is taken from the ground state absorption spectrum. Similarly, the photostationary LE and ICT fluorescence spectra (Figure 1) are converted into the corresponding SE bands. The relative contribution of the BL and the SE(LE) band at time zero and the SE(ICT) band at time infinity can be defined from the ratio of the absolute values for their cross sections (Table 4). The BL scaling is then adjusted in such a way that the remaining ESA spectrum is smooth and positive over the entire probe range. The ESA spectra in Figures 11−15 then result from subtraction of the BL and the SE bands from the overall transient absorption spectra at each time.

Transient Absorption Spectra of ABN in Acetonitrile (260−680 nm). The transient absorption spectrum of ABN in MeCN ($\lambda_{exc} = 290$ nm) between 260 and 680 nm is depicted in Figure 11a, together with the bleach band and the stimulated emission spectrum SE(LE) of the LE state. By the decomposition procedure outlined in the previous section, the ESA spectrum is obtained (Figure 11b), for pump−probe delay times between 0.5 and 68 ps. The LE spectrum has maxima at 295, 320, 445−465, and above 650 nm (see Table 5). The band integral BI(268−283) over the bleach band between 268 and 283 nm decays with a time τ_R of 7.8 ps (insert in Figure 11a, not at magic angle), the rotational reorientation time of ABN in MeCN (Table 5). There is no indication for an ICT reaction for ABN in MeCN over the time range investigated.

Transient Absorption Spectra of DMABN in *n*-Hexane (260−680 nm). The transient absorption spectra of DMABN in *n*-hexane ($\lambda_{exc} = 290$ nm) in Figure 12 show the spectral evolution over the time range 0.5−68 ps. The ESA spectrum of the LE state has maxima at 300, 340, 450, 535, and above 660 nm (Table 5). As with ABN in MeCN (Figure 11), there is no indication for the occurrence ICT, although the process takes place to a small extent as concluded from the appearance of a weak ICT band in the fluorescence spectrum of DMABN in *n*-hexane.[32,85] Instead, the observed spectral changes are uniform in amplitude across the observation range. As pump and probe polarizations were parallel for the measurements, this amplitude decay can be assigned to rotational diffusion of DMABN. The band integral between the wavelengths α and ω is defined as $BI(\alpha - \omega) = \int_{\alpha}^{\omega} \Delta OD(\lambda)\lambda^{-1}\, d\lambda$. From the decay of the band integral BI(270−295) for the bleached ground state absorption between 270 and 295 nm (see insert in Figure 12a), a rotational diffusion time τ_R of 7.4 ps is obtained.

Transient Absorption Spectra of DMABN in Acetonitrile (260−680 nm). Transient absorption spectra ($\lambda_{exc} = 290$ nm) of DMABN in MeCN are displayed in Figure 13a, for pump−probe delays times from 0.2 to 64 ps. The band with a negative

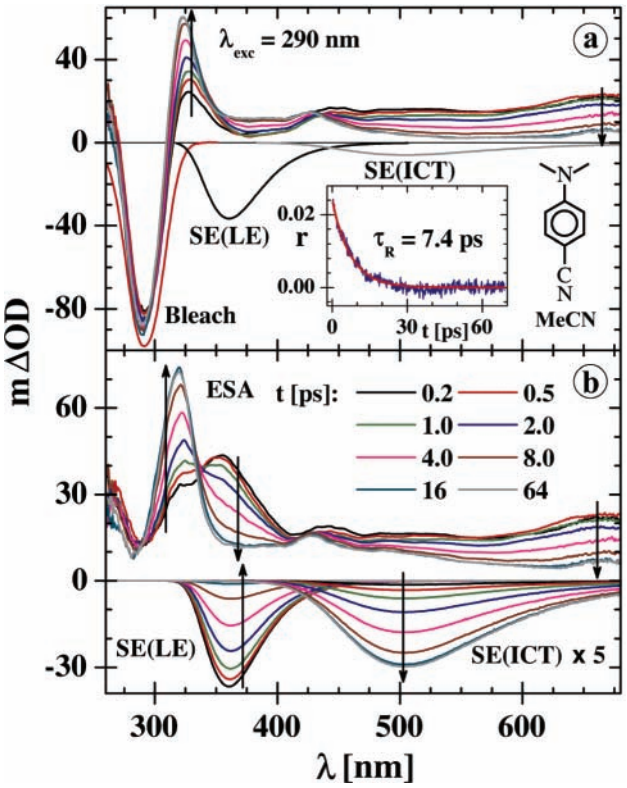

Figure 13. (a) Transient absorption spectra (260−680 nm) of 4-(dimethylamino)benzonitrile (DMABN) in acetonitrile (MeCN) for pump−probe delay times between 0.2 and 64 ps at λ_{exc} = 290 nm. The bleach band and the stimulated emission spectra SE(LE) and SE(ICT) are also displayed. (b) Time development of the excited state absorption (ESA) spectra. The anisotropy r (275−375 nm) decays with a time constant τ_R = 7.4 ps, inset (Table 5), caused by rotational diffusion of DMABN. The rise of the ICT absorption band (320 nm) and the decay of the LE band (355 and above 625 nm) is indicated with an arrow. This time evolution is due to the ICT reaction. The spectrum at a delay of 0.2 ps is effectively that of the LE state. At larger delays, the ESA spectrum develops into that of the ICT state at a delay of 64 ps. mΔOD is the change in optical density/1000.

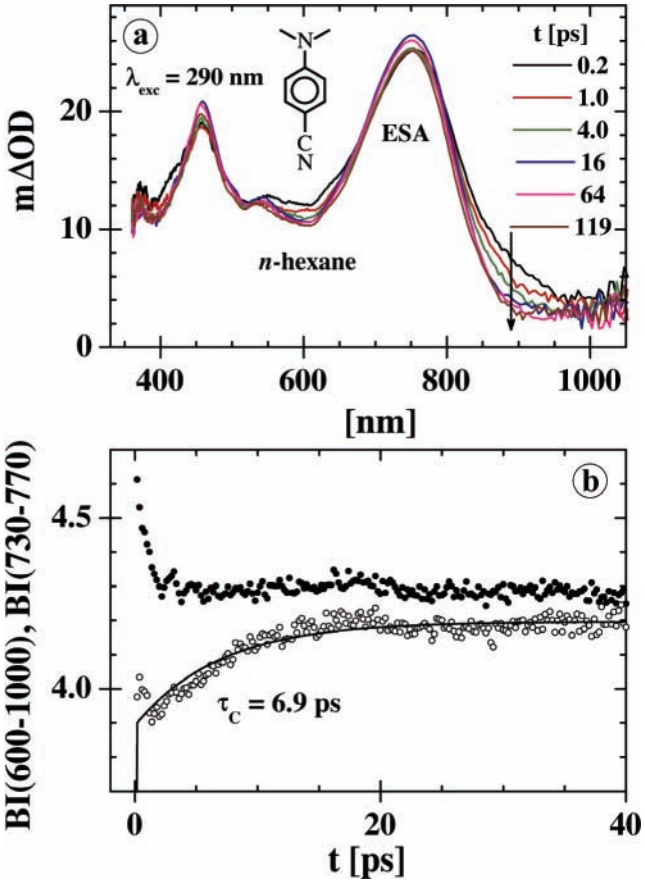

Figure 14. Excited state absorption (ESA) spectra (320−1040 nm) of 4-(dimethylamino)benzonitrile (DMABN) in *n*-hexane at 290 nm excitation, for six pump−probe delay times between 0.2 and 119 ps. In (b), the time development of the band integrals BI(730−770) between 730 and 770 nm (open circles) and BI(600−1000) between 600 and 1000 nm (full circles) is shown. The BI(730−770) grows in with a time τ_C of 6.9 ps. The BI(600−1000) is hardly time dependent. mΔOD is the change in optical density/1000.

peak around 290 nm corresponds to bleaching (BL) of the ground state. With increasing time, the signal decays in the long-wavelength (435−680 nm) part of the spectrum and shows a corresponding growing-in over the short-wavelength 310−370 nm range, with an isosbestic point at 430 nm.

After subtraction of the BL and SE contributions, the ESA spectra are obtained (Figure 13b). The ESA spectrum at the shortest delay time (0.2 ps), has maxima at 320 and 355, around 440, and above 680 nm. It may be assigned to the LE state because the LE → ICT reaction takes place with a decay time τ_2 of 4.1 ps (Figure 7, Table 4). This LE spectrum is similar to that of ABN in MeCN (Figure 11) and DMABN in *n*-hexane (Figure 12). Next let us discuss the evolution of the excited state absorption. A growing-in of the ICT band is observed at 320 nm, whereas a decay of the LE state is seen at 360 and between 450 and 680 nm. All these changes occur with a characteristic time constant τ_2 of around 4 ps. The ESA spectrum at 64 ps delay represents the ICT state, with maxima at 320 and around 430 nm, because at this time the decay of the LE state is essentially complete (τ_2 = 4 ps, Tables 2, 4, and 5). The typical ESA(ICT) peaks at 320 and 430 nm are absent with DMABN in *n*-hexane (Figure 11), indicating that ICT formation does not occur in this system at any delay time. In the range 300−400 nm the LE and ICT bands strongly overlap. A detailed time development of the SE(LE) spectrum is presented in Figure S5 in Supporting Information.

Transient Absorption Spectra (320−1040 nm) at 290 nm. In addition to the 260−680 nm spectra presented in the previous sections, transient absorption spectra were also measured over a wavelength range extended to the red, from 320 to 1040 nm; see Figures 14 and 15.

LE Spectra of DMABN in n-Hexane. The ESA spectra of the LE state of DMABN in *n*-hexane at 290 nm excitation are shown in Figure 14a,b, with the main peaks at around 460 (525) and 750 nm (Table 5). Over the common spectral range (380−680 nm), these spectra are similar to those displayed in Figure 11 (λ_{exc} = 290 nm).

In the ESA spectrum obtained at 290 nm excitation (Figure 14a), the increase of BI(730−770) is relatively small, with a rise time of 6.9 ps; see Figure 14b. The band integral BI(600−1000) over the entire spectral range at both sides of the 750 nm LE absorption peak essentially does not depend on time (Figure 14b). It was reported in ref 85 that the intensity in the transient absorption spectrum (440−740 nm) of DMABN in *n*-hexane increases between 2 and 50 ps after 267 nm excitation, which growth was attributed to a reverse ICT → LE reaction from an endothermic ICT state, formed directly from the S_2 state, bypassing the equilibrated LE state.[8,85] Upon excitation of DMABN in *n*-hexane at 266 nm, a similar increase is found. We interpret this phenomenon in terms of solvent cooling of the excess excitation energy at our 290 nm as compared with the 267 nm in ref 85, and not by a reverse ICT → LE reaction.[8,85] In support of our interpretation, note that in the ESA spectra of

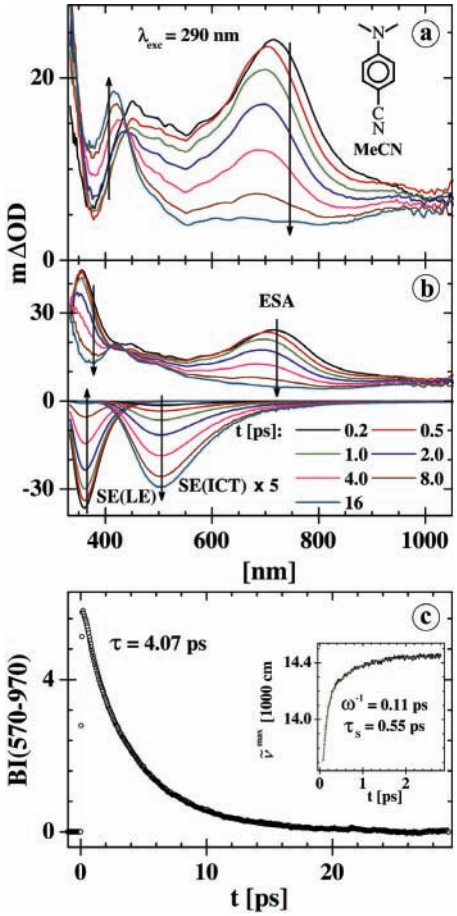

Figure 15. (a) Transient absorption spectra (320−1040 nm) of 4-(dimethylamino)benzonitrile (DMABN) in acetonitrile (MeCN) for seven pump−probe delay times between 0.2 and 16 ps at $\lambda_{exc} = 290$ nm. (b) Time development of the excited state absorption (ESA) spectra and the stimulated emission (SE) spectra of the LE and ICT states. (c) Decay of the band integral BI(570−970) over the LE band between 570 and 970 nm. The decay can be fitted with a single time: 4.07 ps. This time is for the LE → ICT reaction. Inset: shift of the maximum $\tilde{\nu}^{max}$ of the LE(ESA) band around 700 nm, fitted with the expression $\tilde{\nu}^{max}(t) = \tilde{\nu}^{max}(\infty) + a_1 \exp(-{}^1/_2\omega^2t^2) + a_2 \exp(-t/\tau_s)$, in which ω^{-1} and τ_s are the solvation times. The results are $a_1 = -480$ cm^{-1} (0.54), $a_2 = -410$ cm^{-1} (0.46), and $\tilde{\nu}^{max}(\infty) = 14\,450$ cm^{-1}, with the relative contributions in parentheses. mΔOD is the change in optical density/1000.

DMABN in *n*-hexane at early times down to 0.2 ps after 290 nm excitation (Figure 14), there is no indication of an ICT absorption band (maximum at 425 nm, see Figures 13 and 15). In the 260−680 nm ESA spectrum of DMABN in *n*-hexane in Figure 12, in contrast, a decay of the LE bands at 450 and 500−680 nm (0.5−68 ps) is observed. This difference is due to the fact that these spectra were not measured at magic angle.

LE and ICT Absorption of DMABN in Acetonitrile. The transient absorption and the ESA spectra of DMABN in MeCN with $\lambda_{exc} = 290$ nm are displayed in Figure 15a,b, with delay times from 0.2 to 16 ps. The main feature of the ESA spectra is the decay of the LE band: around 700 nm. Also note the rise of the ICT peak at 400 nm in Figure 15a (see Figure 13). The spectrum at 16 ps delay in Figure 15b is that of the ICT state, similar to the one at 64 ps in Figure 13 with peaks at 425 and around 320 nm. The ESA spectrum at the shortest delay time of 0.2 ps, with maxima at 355, around 440 and 680 nm and essentially that of the LE state, is practically the same as that in Figure 13 at 0.2 ps (see Table 5).

The LE band integral BI(570−970) decays with a single time τ_2 of 4.07 ps; see Figure 15c. This time is assigned to the LE → ICT reaction, for which a corresponding time τ_2 of 4.1 ps was obtained for DMABN in MeCN at 25 °C (Table 4 and Figure 7).

The blue shift of the maximum around 710 nm in the LE(ESA) spectrum of DMABN in MeCN for delay times up to 4 ps (see Figure S6 in Supporting Information, taken from Figure 15b) can be fitted as the sum of a Gaussian and an exponential,[98b] with the following times ω^{-1} and τ_2 and amplitudes a_i: $\omega^{-1} = 110$ fs and $\tau_2 = 550$ fs, with relative contributions of 0.54 and 0.46 (Figure 15c). These times and relative amplitudes are similar to those observed for the dielectric relaxation of MeCN determined with coumarine 153 as the probe molecule:[95] 89 fs (0.69) and 630 fs (0.31) from ref 95a and 68 fs (0.70) and 600 fs (0.30) from ref 95b. It is hence concluded that ω^{-1} and τ_2 are the relaxation times of the solvent MeCN.

It has recently been observed for a series of 2,3,5,6-tetrafluoroaminobenzonitriles that the ICT reaction in MeCN is governed by the dielectric solvent relaxation, with a main reaction time of around 90 fs,[96] comparable to the major solvent relaxation times[95] of 89 or 68 fs. The occurrence of large amplitude motions, such as a full 90° twist of a dimethylamino group, is rather unlikely under such conditions. The same conclusion is made here for DMABN in MeCN, based on the development of the ICT peak at 320 nm in the ESA spectrum (Figure 13b), which has reached its final spectral position already at 0.2 ps after excitation.

In summary, intramolecular charge transfer in photoexcited DMABN is measured down to 200 fs at nanometer spectral resolution. The photometric signal/noise ratio allows us to distinguish small fractions (5%) of the population in the excited state. Single-exponential behavior is observed in the early time window <70 ps. The characteristic time constant of 4.1 ps is in excellent agreement with the picosecond SPC results. The transient absorption spectra were quantitatively decomposed into the SE and ESA contributions, both for the LE and for the ICT state. This decomposition should help in quantifying intramolecular charge transfer when, for example, the excess excitation energy is varied.

LE and ICT Absorption Spectra. DMABN in *n*-Hexane (LE) and Acetonitrile (LE and ICT) and ABN in Acetonitrile (LE). The excited state absorption spectra of DMABN in *n*-hexane and MeCN as well as of ABN in MeCN are displayed in Figures 16 and 17. These spectra (260−1040 nm) are constructed from the spectra at the two overlapping spectral ranges, 260−680 and 360−1040 nm in Figures 12−15 for DMABN and in Figures 11 and S7 for ABN.

The ESA spectra of (a) DMABN in *n*-hexane and of (b) ABN in MeCN, shown at pump−probe delay times of 0.4 and 1.0 ps in Figure 16a,b, are both for the LE state (maxima in Table 5).

The ESA spectrum of DMABN in MeCN is depicted for two pump−probe delay times in Figure 17: the spectrum at a delay time of 0.2 ps (a) is that of the LE state and the spectrum at a delay time of 68 ps (b) is that of the ICT state (maxima in Table 5). The LE spectrum of DMABN in MeCN is similar to that in *n*-hexane (Figure 16a). The difference around 300 nm may be due to the presence of overlapping bleach, LE and ICT bands over this range (Figures 13 and 15).

The LE and ICT ESA spectra in Figures 16 and 17 are in good agreement with those reported in the literature over more limited spectral ranges: DMABN (310−740 nm) and ABN (430−720 nm);[7,85,93,94] see Table 5.

TABLE 5: Excited State Absorption (ESA) Maxima, Rotational Relaxation Times τ_R, ICT Decay Times τ_2, Solvent Cooling Times τ_C and Solvent Relaxation Times ω^{-1} and τ_S for 4-Aminobenzonitrile (ABN) and 4-(Dimethylamino)benzonitrile (DMABN) in Acetonitrile (MeCN) and *n*-Hexane

	ESA maxima (nm)		decay times τ_R and τ_2(ICT), (λ_{exc}) (ps)	
	MeCN	*n*-hexane	MeCN	*n*-hexane
ABN	298, 320, 445−472, 685 (LE), Figure 16b 450−475 (ref 7)[b]	465, 660−720 (LE), Figure S7c 480 (ref 7)[b]	7.8 (τ_R)[a]	
DMABN	320, 355, 440, 710 (LE), Figure 17a 315, 425, (490), 970 (ICT), Figure 17b	300, 320, 445, 470, 745 (LE) Figure 16a	7.4 (τ_R)[c] 4.07 (τ_2, 290 nm)[d] 0.11 (ω^{-1})[f] 0.55 (τ_S)[f]	7.4 (τ_R)[a] 6.9 ps (τ_C) (290 nm)[e]
	420 (ICT) (ref 94),[g] 325, 400 (ICT) (ref 93)[i]	460, 525, 710 (LE) (refs 7, 85)[h]		

[a] Rotational relaxation time measured over the bleach band between 270 and 295 nm in the transient spectra (see Figure 11). [b] Spectral range: 430−720 nm. [c] From anisotropy decay in the bleach band (275−305 nm). [d] Decay of the LE(ESA) band; see Figure 15c. [e] The time τ_C is attributed to solvent cooling; see text (Figure 14c). [f] See Figure 15c. [g] Spectral range: 380−600 nm. [h] Spectral range: 440−740 nm (ref 85). [i] Spectral range: 310−480 nm.

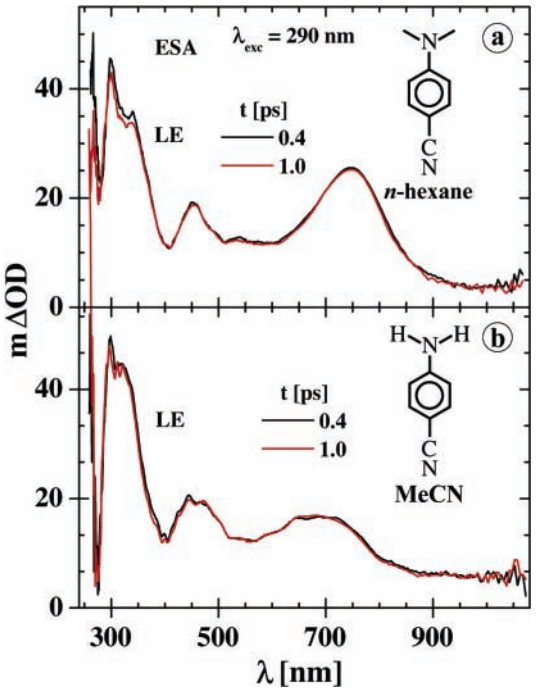

Figure 16. Excited state absorption (ESA) spectra (260−1040 nm) of (a) 4-(dimethylamino)benzonitrile (DMABN) in *n*-hexane and (b) 4-aminobenzonitrile (ABN) in acetonitrile (MeCN) at 290 nm excitation for two pump−probe delay times. The spectra are for the LE state of DMABN and ABN. See text, Figures 12 and 15 for DMABN and Figures 11 and S7 for ABN. mΔOD is the change in optical density/1000.

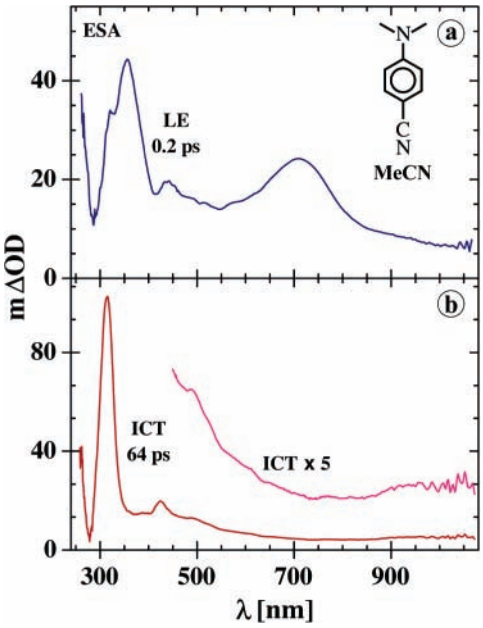

Figure 17. Excited state absorption (ESA) spectra (260−1040 nm) of 4-(dimethylamino)benzonitrile (DMABN) in acetonitrile (MeCN) at 290 nm excitation for two pump−probe delay times: (a) the spectrum at a delay time of 0.2 ps for the LE state and (b) that at a delay time of 68 ps for the ICT state. See text and Figures 13 and 15. mΔOD is the change in optical density/1000.

Conclusion

The ICT reaction of DMABN in MeCN was studied as a function of temperature, by measuring fluorescence spectra and quantum yields together with picosecond fluorescence decays over the range between −45 and +75 °C. From these experiments, the kinetic and thermodynamic reaction parameters can be determined. Formation of the photoproduct MABN, however, makes a sufficiently precise measurement of the ICT → LE back reaction from the LE fluorescence decay impossible, as the LE fluorescence is strongly quenched for DMABN in MeCN and is hence affected by small amounts of photoproduct. Therefore, a simultaneous analysis of the LE fluorescence decays, the LE and ICT fluorescence quantum yields, the data for the longest decay time τ_1 and the lifetime τ_0 of the model compound MABN was undertaken. This analysis was carried out with the following constraints: the Arrhenius expression holds for the forward and backward ICT rate constants k_a and k_d and the temperature dependence of the LE radiative rate constant k_f only depends on n^2. In this manner, the detrimental effect of photoproduct formation could be overcome. From k_a and k_d so obtained as a function of temperature, their activation energies E_a (5.0 kJ/mol) and E_d (32.0 kJ/mol) and preexponential factors k_a^0 (1.8×10^{12} s^{-1}) and k_d^0 (190×10^{12} s^{-1}) were determined, giving the ΔH (−27.0 kJ/mol) and ΔS [−38 J/(mol K)] for the ICT reaction. The activation barrier E_a of 5 kJ/mol means that the ICT process of DMABN in MeCN is not a barrierless reaction. As the dielectric constant of MeCN changes with temperature, the barrier E_a also will depend on temperature, approximately decreasing from 6 to 4 kJ/mol between +75 and −45 °C. When the photoproduct is neglected, in particular the data involving k_d are affected, with the following not optimal results: E_d (23 kJ/mol), ΔH (−18 kJ/mol), and ΔS

[−15 J/(mol K)]. It is also found that the ratio of the ICT and LE radiative rates k'_f(ICT)/k_f(LE) as well as the ICT lifetime τ'_0(ICT) depend on temperature.

Femtosecond transient absorption, ESA, and SE spectra of DMABN and ABN in *n*-hexane and MeCN were measured over the range 260 to 1040 nm, with pump−probe delay times between 0.2 and 119 ps, at an excitation wavelength of 290 nm. For DMABN in *n*-hexane as well as for ABN in *n*-hexane, the ESA spectrum is that of the LE state, without, in the case of DMABN, any indication of the presence of an ICT state. The bleach spectra show a decay with a time τ_R of 7.4 ps for DMABN and 7.8 ps for ABN, attributed to rotational diffusion of the aminobenzonitriles. For DMABN in *n*-hexane at 267 nm excitation, an increase with time in signal intensity has been observed in the literature for the LE(ESA) spectrum. This increase is considerably smaller at our 290 nm excitation. We therefore attribute this former rise in signal intensity to relaxation of the excess excitation energy by solvent cooling, contrary to an interpretation in the literature that the phenomenon is due to a reverse ICT → LE reaction from an endothermic ICT state formed directly from the S_2 state, bypassing the equilibrated LE state. In support of our explanation, note that an indication of the presence of the ICT state is not found in our subpicosecond ESA spectra of DMABN in *n*-hexane. For DMABN in MeCN, the ESA spectrum strongly changes with time, due to the ICT reaction. At a delay time of 0.2 ps, the spectrum is essentially that of the LE state, with maxima at 320−360, 450, and 710 nm. This spectrum changes with a time constant of 4.07 ps (λ_{exc} = 290 nm) into that of the ICT state, with a main maximum at 320 nm and a smaller peak at 430 nm. From the picosecond LE and ICT fluorescence decays the same time τ_2 of 4.1 ps is obtained. The sharp ICT(ESA) peak at 320 nm does not change its spectral position after a pump−probe delay time of 0.2 ps, which indicates that large amplitude motions do not take place after this time.

Acknowledgment. Many thanks are due to Mr. Jürgen Bienert for carrying out the HPLC purifications and to Mr. Wilfried Bosch and Mr. Helmut Lesche for technical support.

Supporting Information Available: Table of activation and reaction energies, figures of fluorescence, absorption, and emission spectra, graph of rate constants vs refractive index, and textual description of the time evolution of the stimulated LE and ICT emission spectra of DMABN in MeCN. This material is available free of charge via the Internet at http://pubs.acs.org.

References and Notes

(1) Lippert, E.; Lüder, W.; Boos, H. In *Advances in Molecular Spectroscopy*; European Conference on Molecular Spectroscopy, Bologna, Italy, 1959; Mangini, A., Ed.; Pergamon Press: Oxford, U.K., 1962; p 443.

(2) Lippert, E.; Lüder, W.; Moll, F.; Nägele, W.; Boos, H.; Prigge, H.; Seibold-Blankenstein, I. *Angew. Chem.* **1961**, *73*, 695.

(3) Rettig, W. *Angew. Chem., Int. Ed. Engl.* **1986**, *25*, 971.

(4) (a) Leinhos, U.; Kühnle, W.; Zachariasse, K. A. *J. Phys. Chem.* **1991**, *95*, 2013. (b) Il'ichev, Yu. V.; Kühnle, W.; Zachariasse, K. A. *J. Phys. Chem. A* **1998**, *102*, 5670.

(5) Lommatzsch, U.; Brutschy, B. *Chem. Phys.* **1998**, *234*, 35.

(6) Okamoto, H.; Inishi, H.; Nakamura, Y.; Kohtani, S.; Nakagaki, R. *J. Phys. Chem. A* **2001**, *105*, 4182.

(7) Ma, C.; Kwok, W. M.; Matousek, P.; Parker, A. W.; Phillips, D.; Toner, W. T.; Towrie, M. *J. Phys. Chem. A* **2002**, *106*, 3294.

(8) Fuss, W.; Pushpa, K. K.; Rettig, W.; Schmid, W. E.; Trushin, S. A. *Photochem. Photobiol. Sci.* **2002**, *1*, 255.

(9) Grabowski, Z. R., Rotkiewicz, K., Rettig, W. *Chem. Rev.* **2003**, *103*, 3899.

(10) Yoshihara, T.; Galievsky, V. A.; Druzhinin. S. I.; Saha, S.; Zachariasse, K. A. *Photochem. Photobiol. Sci.* **2003**, *2*, 342.

(11) Zachariasse, K. A.; Druzhinin, S. I.; Bosch, W.; Machinek, R. *J. Am. Chem. Soc.* **2004**, *126*, 1705.

(12) Serrano-Andrés, L.; Merchán, M.; Roos, B. O.; Lindh, R. *J. Am. Chem. Soc.* **1995**, *117*, 3189.

(13) Parusel, A. B. J.; Köhler, G.; Nooijen, M. *J. Phys. Chem. A* **1999**, *103*, 4056.

(14) Sudholt, W.; Sobolewski, A. L.; Domcke, W. *Chem. Phys.* **1999**, *250*, 9.

(15) Dreyer, J.; Kummrow, A. *J. Am. Chem. Soc.* **2000**, *122*, 2577.

(16) Zilberg, S.; Haas, Y. *J. Phys. Chem. A* **2002**, *106*, 1.

(17) Jamorski Jödicke, C.; Lüthi, H. P. *J. Chem. Phys.* **2003**, *119*, 12852.

(18) Rappoport, D.; Furche, F. *J. Am. Chem. Soc.* **2004**, *126*, 1277.

(19) Köhn, A.; Hättig, C. *J. Am. Chem. Soc.* **2004**, *126*, 7399.

(20) Zachariasse, K. A.; Yoshihara, T.; Druzhinin. S. I. *J. Phys. Chem. A* **2002**, *106*, 6325. Erratum: *J. Phys. Chem. A* **2002**, *106*, 8978.

(21) Rotkiewicz, K.; Grellmann, K. H.; Grabowski, Z. R. *Chem. Phys. Lett.* **1973**, *19*, 315.

(22) Khalil, O. S.; Hofeldt, R. H.; McGlynn, S. P. *Chem. Phys. Lett.* **1972**, *17*, 479.

(23) Rotkiewicz, K.; Grabowski, Z. R.; Krówczyński, A.; Kühnle, W. *J. Luminescence* **1976**, *12/13*, 877.

(24) Kosower, E. M.; Dodiuk, H. *J. Am. Chem. Soc.* **1976**, *98*, 924.

(25) Siemiarczuk, A.; Grabowski, Z. R.; Krówczyński, A.; Asher, M.; Ottolenghi, M. *Chem. Phys. Lett.* **1977**, *51*, 315.

(26) Visser, R. J.; Varma, C. A. G. O. *J. Chem. Soc., Faraday Trans. 2* **1980**, *76*, 453.

(27) Cazeau-Dubroca, C.; Peirigua, A.; Ait Lyazidi, S.; Nouchi, G. *Chem. Phys. Lett.* **1983**, *98*, 511.

(28) Gorse, A.-D.; Pesquer, M. *J. Phys. Chem.* **1995**, *99*, 4039.

(29) Sobolewski, A. L.; Domcke, W. *Chem. Phys. Lett.* **1996**, *250*, 428.

(30) Zachariasse, K. A.; von der Haar, Th.; Hebecker, A.; Leinhos, U.; Kühnle, W. *J. Photochem. Photobiol. A: Chem.* **1997**, *105*, 373.

(31) In the listing presented here, the first publication in which a particular suggestion is established as a model is taken. A possible twisting of the amino group of DMABN was already suggested in 1973 (ref 21), whereas the TICT model as such first appeared in 1977; see refs 23 and 25. Similarly, Schuddeboom et al.[32] discussed a change from planar to pyramidal hybridization of the amino nitrogen in the ICT state of DMABN as a possible alternative to either TICT or a structural deformation of the phenyl ring, although the corresponding WICT model was introduced by Gorse and Pesquer at a later stage.[28] The suggestion of an exciplex with the solvent was made by Nakashima and Mataga[33] (electrostatic complex with polar molecules, including self-complex formation) as well as by Chandross.[34]

(32) Schuddeboom, W.; Jonker, S. A.; Warman, J. M.; Leinhos, U.; Kühnle, W.; Zachariasse, K. A. *J. Phys. Chem.* **1992**, *96*, 10809.

(33) Nakashima, N.; Mataga, N. *Bull. Chem. Soc. Jpn.* **1973**, *46*, 3016.

(34) Chandross, E. A. In *The Exciplex*; Gordon, M., Ware, W. R., Eds.; Academic Press: New York, 1975; p 187.

(35) Grabowski, Z. R.; Dobkowski, J. *Pure Appl. Chem.* **1983**, *55*, 245.

(36) Yoshihara, T.; Druzhinin, S. I.; Zachariasse, K. A. *J. Am. Chem. Soc.* **2004**, *126*, 8535.

(37) Techert, S.; Zachariasse, K. A. *J. Am. Chem. Soc.* **2004**, *126*, 5593.

(38) Rotkiewicz, K.; Grabowski, Z. R.; Jasny, J. *Chem. Phys. Lett.* **1975**, *34*, 55.

(39) Takagi, Y.; Sumitani, M.; Yoshihara, K. *Rev. Sci. Instrum.* **1981**, *52*, 1003.

(40) Huppert, D.; Rand, S. D.; Rentzepis, P. M.; Barbara, P. F.; Struve, W. S.; Grabowski, Z. *J. Chem. Phys.* **1981**, *75*, 5714.

(41) Zachariasse, K. A.; Grobys, M.; von der Haar, Th.; Hebecker, A.; Il'ichev, Yu. V.; Jiang, Y.-B.; Morawski, O.; Kühnle, W. *J. Photochem. Photobiol. A: Chem.* **1996**, *102*, 59. Erratum: *J. Photochem. Photobiol. A: Chem.* **1998**, *115*, 259.

(42) von der Haar, Th.; Hebecker, A.; Il'ichev, Yu. V.; Kühnle, W.; Zachariasse, K. A. *Fast Elementary Processes in Chemical and Biological Systems*; Lille, France, 1995; AIP Conference Proceedings; AIP: Melville, NY, 1996; No. 364, p 295.

(43) Changenet, P.; Plaza, P.; Martin, M. M.; Meyer, Y. H. *J. Phys. Chem. A* **1997**, *101*, 8186.

(44) Somewhat different values were found for τ_1 and A: 3.12 ns and 10 (ref 42), 2.9 ns and 49 or 99 (ref 43).

(45) (a) Geggier, P.; Zachariasse, K. A. Unpublished results. (b) Geggier, P., Diplomarbeit (Master Thesis), University of Göttingen, 1996.

(46) The fluorescence decays of DMABN have been measured as a function of temperature in a series of alkyl cyanides, from *n*-undecyl cyanide to MeCN (ref 45). It was found that the shortest decay time τ_2 decreases in this series with increasing solvent polarity. For τ_2 in MeCN, a value of 6 ps was found,[41,42] the same value as already obtained in the less polar solvent *n*-propyl cyanide, indicating that τ_2 in MeCN must in fact be shorter than

6 ps. The problem was attributed to photoproduct formation.[41,42] The difference with the measurements presented in the present paper is in part due to the optimization of the picosecond laser SPC setup (shorter excitation duration, made possible by increased picosecond laser system stability; MCP Hamamatsu R3809 instead of R2809U) but mainly comes from a substantial reduction of photoproduct formation. See text.

(47) Hicks, J.; Vandersall, M.; Babarogic, Z.; Eisenthal, K. B. *Chem. Phys. Lett.* **1985**, *116*, 18.

(48) Hicks, J. M.; Vandersall, M. T.; Sitzmann, E. V.; Eisenthal, K. B. *Chem. Phys. Lett.* **1987**, *135*, 413.

(49) Leinhos, U. Ph.D. Thesis, University of Göttingen, Germany, 1991.

(50) Kovalenko, S.; Zachariasse, K. A. Unpublished results.

(51) Yoshihara, T.; Druzhinin. S. I.; Demeter, A.; Kocher, N.; Stalke, D.; Zachariasse, K. A. *J. Phys. Chem. A* **2005**, *109*, 1497.

(52) Chudoba, C.; Kummrow, A.; Dreyer, J.; Stenger, J.; Nibbering, E. T. J.; Elsaesser, T.; Zachariasse, K. A. *Chem. Phys. Lett.* **1999**, *309*, 357.

(53) Phillips, D. *Spectrum* **2002**, *15*, 8.

(54) Kwok, W. M.; George, M. W.; Grills, D. C.; Ma, C.; Matousek, P.; Parker, A. W.; Phillips, D.; Toner, W. T.; Towrie, M. *Angew. Chem., Int. Ed. Engl.* **2003**, *42*, 1826.

(55) Koti, A. S. R.; Periasamy, N. *Res. Chem. Intermed.* **2002**, *28*, 831.

(56) Iwase, E.; Tomioka, A.; Saigusa, H.; Yagi, M. *Phys. Chem. Chem. Phys.* **2004**, *6*, 3852.

(57) Dedonder-Lardeux, C.; Jouvet, C.; Martrenchard, S.; Solgadi, D.; McCombie, J.; Howells, B. D.; Palmer, T. F.; Subaric-Leitis, A.; Monte, C.; Rettig, W.; Zimmermann, P. *Chem. Phys.* **1995**, *191*, 271.

(58) Peng, L. W.; Dantus, M.; Zewail, A. H.; Kemnitz, K.; Hicks, J. M.; Eisenthal, K. B. *J. Phys. Chem.* **1987**, *91*, 6162.

(59) (a) Warren, J. A.; Bernstein, E. R.; Seeman, J. I. *J. Chem. Phys.* **1988**, *88*, 871. (b) Shang, Q.-Y.; Bernstein, E. R. *J. Chem. Phys.* **1992**, *97*, 60. (c) Bernstein, E. R. *J. Phys. Chem.* **1992**, *96*, 10105.

(60) Howell, R.; Phillips, D.; Petek, H.; Yoshihara, K. *Chem. Phys.* **1994**, *188*, 303.

(61) Krauss, O.; Lommatzsch, U.; Lahmann, C.; Brutschy, B.; Rettig, W.; Herbich, J. *Phys. Chem. Chem. Phys.* **2001**, *3*, 74.

(62) Saigusa, H.; Iwase, E.; Nishimura, M. *J. Phys. Chem.* **2003**, *107*, 3759.

(63) Saigusa, H.; Iwase, E.; Nishimura, M. *J. Phys. Chem.* **2003**, *107*, 4989.

(64) Polimeno, A.; Barbon, A.; Nordio, P. L.; Rettig, W. *J. Phys. Chem.* **1994**, *98*, 12158.

(65) (a) Hayashi, S.; Ando, K.; Kato, S. *J. Phys. Chem.* **1995**, *99*, 955. (b) Kato, S.; Amatatsu, Y. *J. Chem. Phys.* **1990**, *92*, 7241. (c) Minezawa, N.; Kato, S. *J. Phys. Chem. A* **2005**, *109*, 5445.

(66) (a) Kim, H. J.; Hynes, J. T. *J. Photochem. Photobiol. A: Chem.* **1997**, *105*, 337. (b) Fonseca, T.; Kim, H. J.; Hynes, J. T. *J. Photochem. Photobiol. A: Chem.* **1994**, *82*, 67. (c) Hynes, J. T. *Rev. Port. Quim.* **1995**, *2*, 12.

(67) Gorse, A.-D.; Pesquer, M. *J. Phys. Chem.* **1995**, *99*, 4039.

(68) (a) Gedeck, P.; Schneider, S. *J. Photochem. Photobiol. A: Chem.* **1999**, *121*, 7. (b) Gedeck, P.; Schneider, S. *J. Photochem. Photobiol. A: Chem.* **1997**, *105*, 165.

(69) (a) Sudholt, W.; Staib, A.; Sobolewski, A. L.; Domcke, W. *Phys. Chem. Chem. Phys.* **2000**, *2*, 4341. (b) Sobolewski, A. L.; Sudholt, W.; Domcke, W. *J. Phys. Chem. A* **1998**, *102*, 2716.

(70) (a) Parusel, A. B. J. *Phys. Chem. Chem. Phys.* **2000**, *2*, 5545. (b) Parusel, A. B. J.; Rettig, W.; Sudholt, W. *J. Phys. Chem. A* **2002**, *106*, 804.

(71) Mennucci, B.; Toniolo, A.; Tomasi, J. *J. Am. Chem. Soc.* **2000**, *122*, 10621.

(72) Gómez, I.; Reguero, M.; Boggio-Pasqua, M.; Robb, M. A. *J. Am. Chem. Soc.* **2005**, *127*, 7119.

(73) (a) Heisel, F.; Miehé, J. A. *Chem. Phys.* **1985**, *98*, 233. (b) Heisel, F.; Miehé, J. A.; Martinho, J. M. G. *Chem. Phys.* **1985**, *98*, 243.

(74) Rettig, W.; Fritz, R.; Braun, D. *J. Phys. Chem. A* **1997**, *101*, 6830.

(75) Bagchi, B.; Fleming, G. R. *J. Phys. Chem.* **1990**, *94*, 9.

(76) Dahl, K.; Biswas, R.; Ito, N.; Maroncelli, M. *J. Phys. Chem. B* **2005**, *109*, 1563.

(77) Druzhinin, S. I.; Galievsky, V. A.; Zachariasse, K. A. *J. Phys. Chem. A*, in press.

(78) Demeter, A.; Zachariasse, K. A. *Chem. Phys. Lett.* **2003**, *380*, 699.

(79) The modification of the Fluoromax-3 spectrofluorometer consists of Peltier cooling to −10 °C of the detector photomultiplier (PMT, Hamamatsu R928P) located in a housing (with external water circuit) outside of the Fluoromax-3. The exit slit of the monochromator is focused on the PMT photocathode by an optimized toric mirror.

(80) Demas, J. N.; Crosby, G. A. *J. Phys. Chem.* **1971**, *75*, 991.

(81) Kovalenko, S. A.; Dobryakov, A. L.; Ruthmann, J.; Ernsting, N. P. *Phys. Rev. A* **1999**, *59*, 2369.

(82) Ernsting, N. P.; Kovalenko, S. A.; Senyuskina, T. A.; Saam, J.; Farztdinov, V. *J. Phys. Chem. A* **2001**, *105*, 3443.

(83) Druzhinin. S. I.; Demeter, A.; Galievsky, V. A.; Yoshihara, T.; Zachariasse, K. A. *J. Phys. Chem. A* **2003**, *107*, 8075.

(84) Zachariasse, K. A.; von der Haar, Th.; Hebecker, A.; Leinhos, U.; Kühnle, W. *Pure Appl. Chem.* **1993**, *65*, 1745.

(85) Kwok, W. M.; Ma, C.; Phillips, D.; Matousek, P.; Parker, A. W.; Towrie, M. *J. Phys. Chem. A* **2000**, *104*, 4188.

(86) Landolt-Börnstein, *Numerical Data and Functional Relationships in Science and Technology*; Madelung, O., Ed.; New Series; Springer: Berlin, 1991; Group IV, Vol. 6.

(87) Sevens, B.; Ban, M. I. *Trans. Faraday Soc.* **1964**, *60*, 1515.

(88) Zachariasse, K. A. *Trends Photochem. Photobiol.* **1994**, *3*, 211.

(89) Grobys, M. Ph.D. Thesis, University of Göttingen, Germany, 1997.

(90) (a) Onsager, L. *J. Am. Chem. Soc.* **1936**, *58*, 1486. (b) Milischuk, A.; Matyushov, D. V. *J. Phys. Chem. A* **2002**, *106*, 2146. (c) Małecki, J. In *Molecular Interactions*; Ratajczak, H., Orville-Thomas, W. J., Eds.; Wiley: Chicester, U.K., 1982; Vol. 3, p 183. (d) Suppan, P.; Ghoneim, N. *Solvatochromism*; The Royal Society of Chemistry: Cambridge, U.K., 1997.

(91) With DMABN in MeCN, $\tilde{\nu}^{max}$(ICT) has the following temperature dependence: 19 460 cm^{-1} (−45 °C), 20 310 cm^{-1} (25 °C), 20 870 cm^{-1} (75 °C): $\Delta\tilde{\nu}^{max}$(ICT) = 1410 cm^{-1} between 75 and −45 °C, whereas $\Delta\tilde{\nu}^{max}$(LE) is much smaller (93 cm^{-1}) over this temperature range. For $\tilde{\nu}^{max}$(ICT) of DIABN in MeCN: 19 940 cm^{-1} (−45 °C), 20 485 cm^{-1} (25 °C), 20 900 cm^{-1} (75 °C), i.e., $\Delta\tilde{\nu}^{max}(ICT)^{75/-45}$ = 960 cm^{-1}, and in *n*-hexane: 25 500 cm^{-1} (−45 °C), 25 800 cm^{-1} (25 °C), 25 930 cm^{-1} (75 °C, extrapolated), i.e., $\Delta\tilde{\nu}^{max}(ICT)^{75/-45}$ = 440 cm^{-1}. The shift of $\tilde{\nu}^{max}$(ICT) for DIABN in *n*-hexane is caused by the temperature dependence of the refractive index *n* (n^{-45} = 1.4127; n^{25} = 1.3724; n^{75} = 1.3420 (ref 92)). The dielectric constant ϵ ($\approx n^2$) of *n*-hexane hardly changes with temperature (ϵ^{-45} = 1.99 to ϵ^{75} = 1.81), in contrast to that of MeCN (ϵ^{-45} = 50.2 to ϵ^{75} = 30.6), from ref 86. The data at 75 °C are extrapolated. We notice that the $\Delta\tilde{\nu}^{max}(ICT)^{75/-45}$ for DMABN in MeCN of 1410 cm^{-1} is considerably larger than the difference in solvation energy (375 cm^{-1} = 4.47 kJ/mol) calculated for the ICT state of DMABN in MeCN between −45 and +75 °C (eq 19). This discrepancy may be due to the fact that $\tilde{\nu}^{max}$(ICT) = *E*(ICT) − *E*(FC) (see eq 4), which means that $\Delta\tilde{\nu}^{max}$(ICT) can to an important extent depend on the temperature dependence of *E*(FC), i.e., on that of the solvent dielectric relaxation.

(92) Landolt-Börnstein. *Numerical Data and Functional Relationships in Science and Technology*; Lechner, M. D., Ed.; New Series; Springer: Berlin, 1996; Group III, Vol. 38B.

(93) (a) Okada, T.; Uesugi, M.; Köhler, G.; Rechthaler, K.; Rotkiewicz, K.; Rettig, W.; Grabner, G. *Chem. Phys.* **1999**, *241*, 327. (b) Okada, T.; Mataga, N.; Baumann, W. *J. Phys. Chem.* **1987**, *91*, 760.

(94) Kwok, W. M.; Ma, C.; George, M. W.; Grills, D. C.; Matousek, P.; Parker, A. W.; Philips, D.; Toner, W. T.; Towrie, M. *Phys. Chem. Chem. Phys.* **2003**, *5*, 1043.

(95) (a) Stratt, R. M.; Maroncelli, M. *J. Phys. Chem.* **1996**, *100*, 12981.(b) Kovalenko, S. A.; Senyushkina, T. A.; Ernsting, N. P. Unpublished results.

(96) Galievsky, V. A.; Druzhinin, S. I.; Demeter, A.; Jiang, Y.-B.; Kovalenko, S. A.; Lustres, L. P.; Venugopal, K.; Ernsting, N. P.; Allonas, X.; Noltemeyer, M.; Machinek, R.; Zachariasse, K. A. *Chem. Phys. Chem.* **2005**, *6*, 2307.